The Astrophysical Journal, 677:1401–1424, 2008 April 20

ATOMIC ALIGNMENT AND DIAGNOSTICS OF MAGNETIC FIELDS IN DIFFUSE MEDIA

Huirong Yan[1] and A. Lazarian[2]

Received 2007 November 6; accepted 2008 January 16

ABSTRACT

We continue our studies of alignment of atoms by radiation in diffuse media and their realignment by the ambient magnetic field. We understand atomic alignment as the alignment of atoms or ions in their ground or metastable states that have more than two fine or hyperfine sublevels. In particular, we consider the alignment in interstellar and circumstellar media, with the goal of developing new diagnostics of magnetic fields in these environments. We provide predictions of the polarization that arises from astrophysically important aligned atoms (ions) with fine structure of the ground level, namely, O I, S II, and Ti II. Unlike our earlier papers which dealt with weak fields only, a part of our current paper is devoted to the studies of atomic alignment when magnetic fields get strong enough to affect the emission from the excited level. This is a regime of the Hanle effect, but modified by the atomic alignment of the atomic ground state. We also discuss the ground Hanle effect where the magnetic splitting is comparable to the pumping rate. Using an example of emission and absorption lines of the S II ion we demonstrate how polarimetric studies can probe magnetic fields in circumstellar regions and accretion disks. In addition, we show that atomic alignment induced by anisotropic radiation can induce substantial variations of magnetic dipole transitions within the ground state, thus affecting abundance studies based on this emission. Moreover, we show that the radio emission arising this way is polarized, which provides a new way to study magnetic fields, e.g., at the epoch of universe reionization.

Subject headings: atomic processes — magnetic fields — polarization

Online material: color figures

1. INTRODUCTION

Magnetic fields have important or dominant effects in many areas of astrophysics, but have been very difficult to quantify. We believe that atomic alignment is a new promising way of studying magnetic fields in radiation-dominated environments. In fact, this diagnostic is far more sensitive than those based on the Zeeman effect. The basic idea of atomic alignment is simple: consider *atoms* or *ions* irradiated by a nearby star and embedded in a magnetic field. Anisotropic radiation pumps the atoms differentially from different magnetic sublevels, resulting in over- or underpopulations of the atomic states of various magnetic quantum numbers, M. The non-LTE populations produce observable polarization in the absorption or emission lines involved in the interaction. The sensitivity of aligned atoms to magnetic field arises from atoms precessing in the magnetic field. It is obvious that to be sensitive to weak magnetic fields, the atomic level should be long lived. The ground and metastable atomic levels with fine and hyperfine structures correspond to this requirement. As a result, these species are the focus of our study.

This paper is the third in the series of papers where we study atomic alignment. Rigorously speaking, ''atomic alignment'' means that the angular momentum of the atoms is not distributed isotropically: in ''fluorescent alignment'' this is due to angular momentum pumping by anisotropic illuminating light; ''magnetic realignment'' occurs when this alignment is modified by precession in a magnetic field. In this paper, however, we use, whenever this does not cause confusion, the terms ''alignment'' and ''realignment'' interchangeably. In Yan & Lazarian (2006, hereafter YL06) we dealt with polarization of absorption lines of the atoms (ions) having fine splitting, while in Yan & Lazarian (2007, hereafter YL07) we dealt with polarization of absorption and emission lines arising from atoms (ions) with hyperfine splitting. Although both papers were focused on developing new techniques for studying magnetic fields in diffuse media, in both papers we discussed other effects of atomic alignment, e.g., the variations of absorption and emission intensities induced by atomic alignment. We showed that atomic alignment opens wide avenues for studies of weak magnetic fields, i.e., fields $\lesssim 10^{-5}$ G, which makes it a unique tool for magnetic field studies in many diffuse astrophysical environments. In YL06 and YL07 we discussed cases of interplanetary, interstellar, circumstellar, and extragalactic studies employing atomic alignment.

In this paper we, first of all, fill in the gap and discuss the polarization of emission lines from atoms (ions) with fine splitting. As in our earlier papers, we show that this provides a technique to study the *geometry* of weak magnetic fields. Similar to our earlier papers, henceforth, for the sake of simplicity, we talk about *atomic alignment* and alignment of *atoms* even when we deal with *ions*. More importantly, we discuss particular regimes that are also sensitive to the magnetic field intensity.

It is well known that magnetic fields play essential roles in the dynamics of circumstellar disks and have a strong influence on the evolution of pre-main-sequence stars, on accretions, outflows, stellar winds, etc. Magnetically controlled accretion has been confirmed for the low-mass T Tauri stars (see Bertout 1989; Camenzind 1990; Königl 1991; Cameron & Campbell 1993; Shu et al. 1994; Johns-Krull et al. 1999). For intermediate-mass stars, particularly Herbig Ae/Be stars, it is believed that a global magnetic field with a complex configuration is responsible for various peculiar phenomena observed for Herbig stars (e.g., Hubrig et al. 2007). For massive stars, magnetic field affects the stellar wind and causes substantial deviation from the spherical geometry (see Ignace et al. 1999). The Zeeman

[1] Canadian Institute for Theoretical Astrophysics, 60 St. George Street, Toronto, ON M5S 3H8, Canada; yanhr@cita.utoronto.ca.
[2] Department of Astronomy, University of Wisconsin, 475 North Charter Street, Madison, WI 53706; alazarian@wisc.edu.

TABLE 1
Relevant Rates for Atomic Alignment

ν_L (s^{-1})	τ_R^{-1} (s^{-1})	A (s^{-1})	A_m (s^{-1})	τ_c^{-1} (s^{-1})
$88(B/5\ \mu G)$	$7.4\times10^5(R_*/r)^2$	2.8×10^8	2.3×10^{-6}	$6.4[(n_e/0.1\ cm^{-3})(8000\ K/T)^{1/2}]\times10^{-9}$

Notes.—We have that ν_L is the Larmor precession rate, τ_R^{-1} is the absorption rate, A is the emission rate of the permitted line, and A_m is the magnetic dipole emission rate for transitions among J levels of the ground state of an atom. Example values for C II are given, and τ_R^{-1} is calculated for an O-type star, where R_* is the radius of the star radius and r is the distance to the star.

effect, including both Zeeman broadening and the circular polarization, is the main diagnostic adopted by the community. However, the measurements based on the Zeeman effect have serious limitations: first of all, the Zeeman effect is only applicable to very strong magnetic fields $\gtrsim$kG; second, the Zeeman splitting will be smeared out by various line-broadening processes, rotation, winds, accretion, and turbulence, especially in the highly dynamical disks; and moreover, the Zeeman effect requires the geometry of the field to be particularly simple, as, otherwise, there will be significant cancellations of polarization between the Zeeman components.

On the other hand, the spectropolarimetry based on atomic alignment and the Hanle effect does not have these constraints. The Hanle effect can measure magnetic field down to 1 G. And both direction and strength can be measured.[3]

However, if the Hanle effect affects the ground state, again very *weak* magnetic fields can be studied. In this paper we also study the ground state Hanle effect, which takes place when the precession rate gets comparable with the pumping rate of the source. As a result, polarization of both *absorption* and *emission* will be influenced according to the topology and the direction of magnetic field. As far as we know, no *emission* lines from species with fine structure of the ground level have been reported to be observed to emanate from interstellar or circumstellar gas. *Absorption* lines are readily available, however (see Morton 1975). The polarization of absorption lines that we study here is thus currently looking more promising. The lower level Hanle effect had been noticed in the analysis of He I D_3 and Na D_2 polarization for solar prominences (Bommier 1980; Landolfi & Landi Degl'Innocenti 1985). However, given the intense pumping in the solar case, the lower level Hanle regime is not well separated from the Hanle regime. For the weaker pumping by the more distant sources we study here, the lower level Hanle regime becomes distinctive. Moreover, we shall demonstrate a new diagnostic through the lower level Hanle effect with the polarization of *absorption* lines.

Atomic alignment in diffuse media demonstrates a real profusion of interesting physical effects, all of which we cannot cover in this paper. Nevertheless, we briefly touch on an issue of the influence of atomic alignment on the measurements of element abundances, in particular, using magnetic dipole lines. Although physically different, this effect can be calculated with the same formalism as in the rest of the paper, which justifies its discussion within the same publication.

In what follows we outline the different regimes of atomic alignment and Hanle effect in § 2. The basic formalism for studying the problem is described in § 3. Following this, we discuss in § 4 the magnetic realignment regime where complementary studies to YL06 and YL07, namely, on polarized absorption and emission, are provided. The polarizations in both the upper level and lower level Hanle regimes are presented in § 5. The atomic alignment is included there and has a notable influence on the predictions of polarizations. Example studies for a circumstellar disk with poloidal or toroidal magnetic field are performed in § 6. In § 7 we discuss the influence of atomic alignment on radio lines. It is demonstrated that atomic alignment not only modulates the distortion of the cosmic microwave background (CMB) arising from optically pumped lines and therefore affects, e.g., abundance estimates in the early universe, but also causes the line to be polarized, thus suggesting a new promising technique to detect magnetic field in the epoch of reionization. A discussion and summary are provided in, respectively, §§ 8 and 9.

2. BASICS OF ATOMIC ALIGNMENT AND HANLE EFFECT

2.1. *Relevant Rates*

Consider the various rates (see Table 1) involved. Those are (1) the rate of the Larmor precession, ν_L, (2) the rate of the optical pumping, R_F, (3) the rate of collisional randomization, τ_c^{-1}, and (4) the rate of the transition within the ground state, τ_T^{-1}. In many cases $\nu_L > R_F > \tau_c^{-1}, \tau_T^{-1}$. Other relations are possible, however. If $\tau_T^{-1} > R_F$, the transitions within the sublevels of the ground state need to be taken into account and the relative distribution among them will be modified. Since emission is spherically symmetric, the angular momentum in the atomic system is preserved, and thus, alignment persists in this case. In the case $\nu_L < R_F$, the magnetic field does not affect the atomic occupations, and atoms are aligned with respect to the direction of radiation. From the expressions in Table 1, we see, for instance, that magnetic field can realign C II at a distance $r > 0.8$ AU from an O star if the magnetic field strength $\sim5\times10^{-4}$ G.

If the Larmor precession rate ν_L is comparable to any of the other rates, the atomic line polarization becomes sensitive to the strength of the magnetic field. In these situations, it is possible to get information about the *magnitude* of magnetic field. If ν_L gets comparable with the decay rate of the excited state, we get into the regime of the *upper state* Hanle effect. If the rate of ion excitation R_F gets comparable with ν_L, we are in the *ground state* Hanle effect regime. In the Hanle regimes, the plane of polarization is being rotated and the degree of polarization is reduced. Below, we give brief descriptions for each regime (see Fig. 1).

[3] Note that unlike the weak magnetic field regime, which is uniquely relevant to diffuse media, the stronger field regime, i.e., the Hanle regime, is relevant to solar studies. The research into the Hanle effect resulted in an important change of the views on solar chromospheres (see Bommier & Sahal-Brechot 1978; Landi Degl'Innocenti 1983, 1984, 1999; Stenflo & Keller 1997; Trujillo Bueno 1999). Studies of magnetic fields with the Hanle effect that take into account atomic alignment have been successful from the ground and resulted in calls for space-based missions to study the Sun polarization with more lines (Trujillo Bueno et al. 2005).

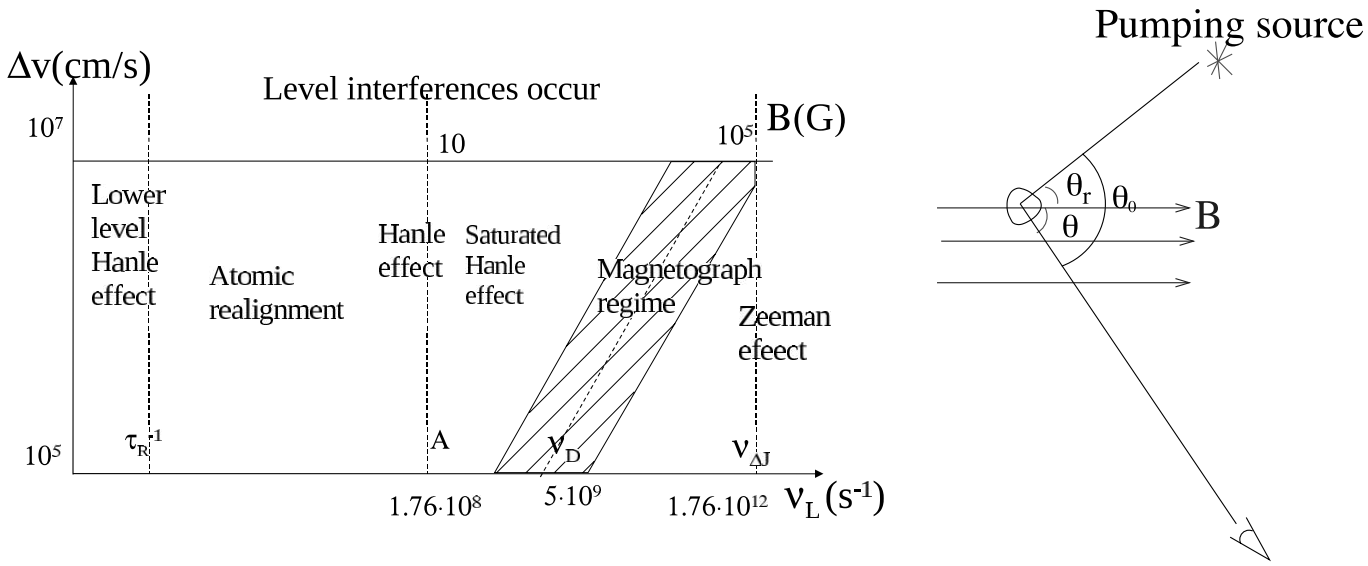

FIG. 1.—Different regimes divided according to the strength of magnetic field and the Doppler line width. Atomic realignment is applicable to weak field (<1 G) in diffuse medium. Level interferences are negligible unless the medium is substantially turbulent ($\delta v \gtrsim 100$ km s^{-1}) and the corresponding Doppler line width becomes comparable to the fine level splitting $\nu_{\Delta J}$. For strong magnetic field, the Zeeman effect dominates. When magnetic splitting becomes comparable to the Doppler width, σ- and π-components (we remind the reader that σ is the circular polarization and π represents the linear polarization) can still distinguish themselves through polarization; this is the magnetograph regime. The Hanle effect is dominant if the Larmor period is comparable to the lifetime of the excited level $\nu_L^{-1} \sim A^{-1}$; similarly, for the ground Hanle effect it requires Larmor splitting to be of the order of the photon pumping rate. For weak magnetic field (<1 G) in diffuse medium, however, atomic alignment is the main effect provided that $\nu_L = 17.6(B/1\ \mu\text{G})\ \text{s}^{-1} > \tau_R^{-1}$. *Right*: Typical astrophysical environment where atomic alignment can happen. A pumping source deposits angular momentum to atoms in the direction of radiation and causes differential occupations on their ground states. In a magnetized medium where the Larmor precession rate ν_L is larger than the photon arrival rate τ_R^{-1}, however, atoms are realigned with respect to magnetic field. Atomic alignment is then determined by θ_r, the angle between the magnetic field and the pumping source. The polarization of the scattered line also depends on the direction of the line of sight, θ and θ_0 (or ϕ, defined further below). [*See the electronic edition of the Journal for a color version of this figure*.]

2.2. *Magnetic Realignment Regime*

We start by discussing a toy model for alignment in which the basic physics is displayed (Varshalovich 1970; Trujillo Bueno et al. 2005; YL06): a two-level atom, with an upper ^1S state (quantum number $J = 0$) and a ^1P ground state, so $J = 1$ (read F for J, for hyperfine structure). Let M be the projection of the atomic angular momentum onto an incident magnetic field, strong enough to dominate the interactions of the atom. For the ground state, M can be -1, 0, and 1, while for the upper state $M = 0$. An incident unpolarized photon beam contains an equal number of left and right circular polarized photons with projected angular momenta of 1 and -1 along the beam. Consider Figure 2, representing atoms viewed along the beam. This radiation coming along the quantization axis will induce transitions only from the $M = -1$ and +1 states, leaving the $M = 0$ ground state overpopulated, since no radiative excitations out of it are possible, while de-excitations into it are. The optical properties of the medium are changed for both polarization and absorption.

For a moderate pumping rate in the circumstellar medium, the magnetic precession is much faster than the pumping (see Table 1); atoms are in this case realigned toward the magnetic field. This can be interpreted both in the *classical* and *quantum* pictures.

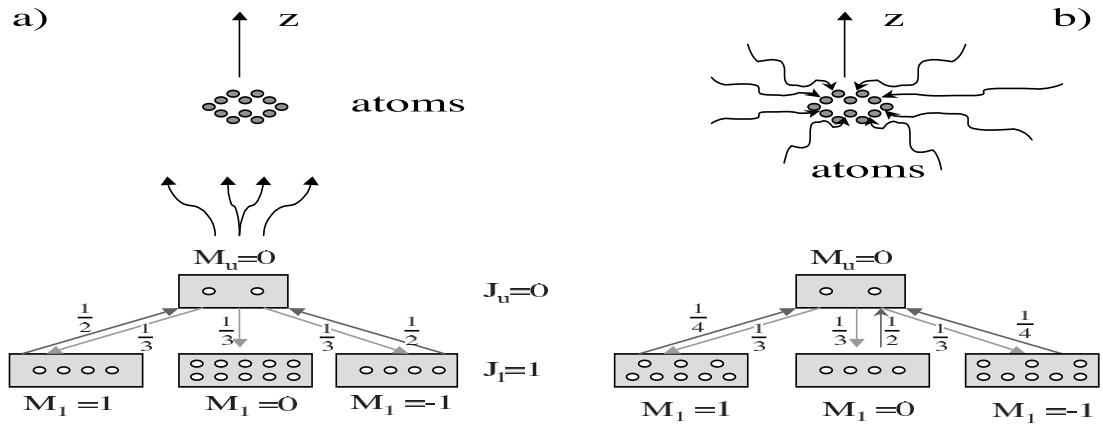

FIG. 2.—Toy model to illustrate how a simple two-level atom is aligned by an incident beam of light. The variable M is the projection of the angular momentum along an incident magnetic field. (*a*) When beam is coming along the direction of $\boldsymbol{B}$ field, atoms accumulate in the ground sublevel $M = 0$, because radiation removes them from the ground states $M = 1$ and -1. Hence, $M = 0$ is overpopulated. (*b*) Incident beam is perpendicular to the $\boldsymbol{B}$ field; $M = \pm 1$ is more populated because the absorptions from sublevels $M = 0$ have higher probabilities, because both right- and left-handed incident polarizations can have projected $M = 0$. [*See the electronic edition of the Journal for a color version of this figure*.]

Owing to the precession, the atoms with different projections of angular momentum will be mixed up. As a result, angular momentum is redistributed among the atoms, and the alignment is altered according to the angle between the magnetic field and radiation field θ_r (see Fig. 1, *right*). This is the *classical* picture.

In the *quantum* picture, if magnetic precession is dominant, then the natural quantization axis will be the magnetic field, which in general is different from the symmetry axis of the radiation. The radiative pumping is to be seen coming from different directions according to the angle between the magnetic field and radiation field θ_r, which results in different alignments.

In the magnetic realignment regime, there is no interference among the magnetic sublevels. And atoms are aligned either parallel or perpendicular to the magnetic field and so are the linear polarization of absorptions from the ground level. The switch of the polarization between the two cases parallel to $\boldsymbol{B}$ ($P > 0$) and perpendicular to $\boldsymbol{B}$ ($P < 0$) happens at the Van Vleck angle $\theta_r = 54.7^\circ$.

2.3. *Hanle Effect*

If the magnetic precession (or splitting) is comparable to the emission rate (or line width A), the polarization is modified according to both the *strength* and the direction of the magnetic field. This is the so-called *Hanle effect* (see, e.g., Stenflo 1994).

Classically, the dipole oscillator will be rotating due to the precession. If the Zeeman splitting $\nu_{\rm L}$ is significantly larger than the line width A (or the inverse of the lifetime of the upper level), the dipole oscillator rotates several times before it gets damped and there is no polarization. However, if the magnetic precession happens at a timescale comparable to the lifetime of the upper level, the dipole oscillator rotates through only a limited angle within the life (or damping) time. As a result, the degree of polarization is both reduced and the polarization plane is rotated compared to the case without magnetic field. The degree and the direction of polarization are determined by both the magnetic field and the direction of observation if the incident light is assumed to be fixed.

In the *quantum* picture, Zeeman splitting lifts the degeneracy among the different magnetic sublevels and, therefore, modifies the interference among the sublevels. This results in the characteristic dependence on magnetic field of the linear polarizations of the emission lines.

Different from the classical picture, the lines have nonzero polarizations in the case of $\nu_{\rm L} \gg A$; this is a regime in which atoms are realigned toward the magnetic field in the excited state before decaying to their ground state. Similar to the "magnetic realignment regime," the polarization of emission is either parallel or perpendicular to the magnetic field and insensitive to the direction of magnetic field. This regime is the "saturated Hanle regime." Note that in the Hanle regime, atoms are also aligned in the ground state, as the magnetic precession period is longer than the lifetime of the ground state, and the ground state alignment affects the polarized signal of the scattered light.

2.4. *Lower Level Hanle Regime*

An analogy can be made between the lower level Hanle effect and the Hanle effect. In places close to a pumping source, the radiative pumping can get comparable to the magnetic precession provided that magnetic field is weak enough. In this case, a similar scenario occurs on the ground state in analogy to the upper level in the Hanle regime. In this situation, coherence appears in the ground state, and as a result, the polarization of absorption does not have a preferential direction unlike in the alignment regime. Polarization of scattered lines is modulated by the magnetic field as well.

3. FORMALISM

The basic equations describing the statistics of atomic density tensors in the aforementioned different regimes are the same (see YL06),

$$\dot{\rho}^k_q(J_u) + i2\pi\nu_{\rm L} g_u q \rho^k_q(J_u) = -\sum_{J_l} A(J_u \rightarrow J_l)\rho^k_q(J_u) + \sum_{J_l k'}[J_l]\left[\delta_{kk'} p_{k'}(J_u, J_l) B_{lu}\bar{J}^0_0 + \sum_{Qq'} r_{kk'}(J_u, J_l, Q, q') B_{lu}\bar{J}^2_Q\right]\rho^{k'}_{-q'}(J_l),$$

$$\dot{\rho}^k_q(J_l) + i2\pi\nu_{\rm L} g_l q \rho^k_q(J_l) = \sum_{J_u} p_k(J_u, J_l)[J_u] A(J_u \rightarrow J_l)\rho^k_q(J_u) - \sum_{J_u, k'}\left[\delta_{kk'} B_{lu}\bar{J}^0_0 + \sum_{Q,q'} s_{kk'}(J_u, J_l, Q, q') B_{lu}\bar{J}^2_Q\right]\rho^{k'}_{-q'}(J_l),$$

where

$$p_k(J_u, J_l) = (-1)^{J_u + J_l + 1}\begin{Bmatrix} J_l & J_l & k \\ J_u & J_u & 1 \end{Bmatrix}, \qquad p_0(J_u, J_l) = \frac{1}{\sqrt{[J_u, J_l]}}, \tag{1}$$

$$r_{kk'}(J_u, J_l, Q, q) = (3[k, k', 2])^{1/2}\begin{Bmatrix} 1 & J_u & J_l \\ 1 & J_u & J_l \\ 2 & k & k' \end{Bmatrix}\begin{pmatrix} k & k' & 2 \\ q & q' & Q \end{pmatrix}, \tag{2}$$

$$s_{kk'}(J_u, J_l) = (-1)^{J_l - J_u + 1}[J_l](3[k, k', 2])^{1/2}\begin{pmatrix} k & k' & 2 \\ q & q' & Q \end{pmatrix}\begin{Bmatrix} 1 & 1 & 2 \\ J_l & J_l & J_u \end{Bmatrix}\begin{Bmatrix} k & k' & 2 \\ J_l & J_l & J_l \end{Bmatrix}. \tag{3}$$

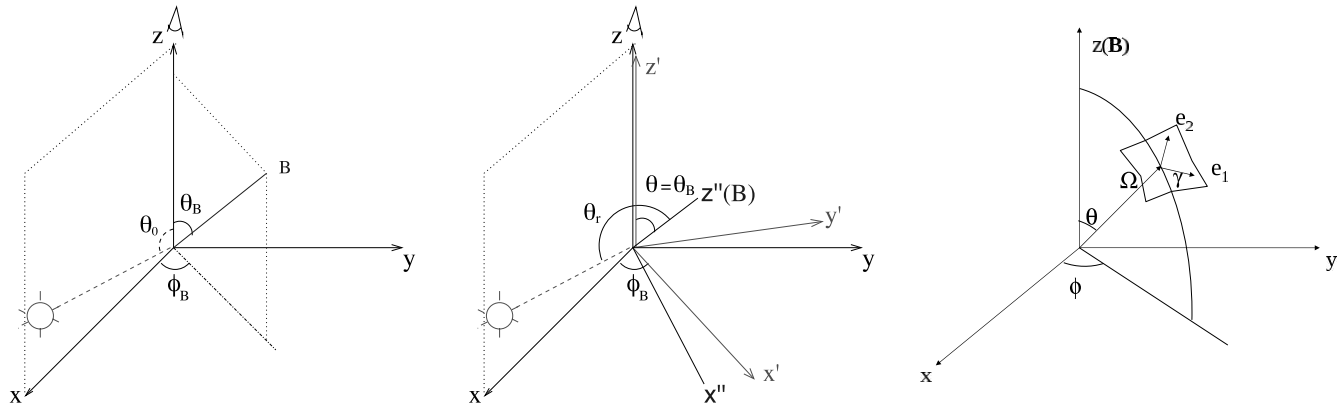

FIG. 3.—*Left*: Geometry of the observational frame. In this frame, the line of sight is the z-axis, and together with the incident light, they specify the x-z plane. Magnetic field is in the (θ_B, ϕ_B)-direction. *Middle*: Transformation to the "theoretical frame" where magnetic field defines the z''-axis. This can be done by two successive rotations specified by Euler angles (ϕ_B, θ_r) (see YL06 for details). The first rotation is from the (x, y, z) coordinate system to the (x', y', z') coordinate system by an angle ϕ_B about the z-axis; the second is from the (x', y', z') coordinate system to the (x'', y'', z'') coordinate system by an angle θ about the y'-axis. Atomic transitions are treated in the "theoretical" frame where the line of sight is in the (θ, π)-direction and the incident radiation is in the (θ_r, ϕ_r)-direction. *Right*: Radiation geometry and the polarization vectors in a given coordinate system; Ω is the direction of radiation. [*See the electronic edition of the Journal for a color version of this figure.*]

In equations (1), ρ^k_q and $\bar{J}^K_Q$ are the irreducible forms of the density matrix of atoms and radiation, respectively. The evolution of the upper state ($\rho^k_q(J_u)$) is represented by equation (1), and the ground state ($\rho^k_q(J_l)$) is described by equation (1). The second terms on the left-hand side of equations (1) represent mixing by magnetic field, where g_u and g_l are the Landé factors for the upper and ground levels, respectively. The two terms on the right-hand side of equation (1) are due to spontaneous emissions and the excitations from the ground level. Transitions to all upper states are taken into account by summing over J_u in equation (1). Vice versa, for an upper level, transitions to all ground sublevels (J_l) are summed up in equation (1). Let us remind our reader that this multilevel treatment is well justified, as level crossing interferences do not exist in the weak field regime unless the medium gets strongly turbulent so that the Doppler width becomes comparable to the energy separation between levels ($\delta v \gtrsim 100$ km s^{-1}, see Fig. 1). The matrix with big curly brackets represents the $6j$ or $9j$ symbol, depending on the size of the matrix. Throughout this paper, we define $[j] \equiv 2j + 1$, which means $[J_l] = 2J_l + 1$, $[J_u] = 2J_u + 1$, etc.

The excitation depends on

$$\bar{J}^K_Q = \int d\nu \frac{\nu_0^2}{\nu^2} \Psi(\nu - \nu_0) \oint \frac{d\Omega}{4\pi} \sum_{i=0}^{3} \mathcal{J}^K_Q(i, \Omega) S_i(\nu, \Omega), \tag{4}$$

which is the radiation tensor of the incoming light averaged over the whole solid angle and the line profile $\Psi(\nu - \nu_0)$. The $S_i = [I, Q, U, V]$ represent the Stokes parameters. In many cases, the radiation source is so far way that it can be treated as a point source. The irreducible unit tensors for Stokes parameters I, Q, and U are

$$\mathcal{J}^0_0(i, \Omega) = \begin{pmatrix} 1 \\ 0 \\ 0 \end{pmatrix}, \qquad \mathcal{J}^2_0(i, \Omega) = \frac{1}{\sqrt{2}} \begin{bmatrix} (1 - 1.5 \sin^2\theta) \\ -3/2 \sin^2\theta \cos 2\gamma \\ 3/2 \sin^2\theta \sin 2\gamma \end{bmatrix}, \qquad \mathcal{J}^2_{\pm 1}(i, \Omega) = \sqrt{3} e^{\pm i\phi} \begin{bmatrix} \mp \sin 2\theta/4 \\ \mp(\sin 2\theta \cos 2\gamma - 2i \sin\theta \sin 2\gamma)/4 \\ \pm(\sin 2\theta \sin 2\gamma - 2i \sin\theta \cos 2\gamma)/4 \end{bmatrix},$$

$$\mathcal{J}^2_{\pm 2}(i, \Omega) = \sqrt{3} e^{\pm 2i\phi} \begin{Bmatrix} \sin^2\theta/4 \\ -[(1 + \cos^2\theta)\cos 2\gamma \mp 2i \cos\theta \sin 2\gamma]/4 \\ [(1 + \cos^2\theta)\sin 2\gamma \mp 2i \cos\theta \cos 2\gamma]/4 \end{Bmatrix}. \tag{5}$$

They are determined by its direction Ω and the reference chosen to measure the polarization (see Fig. 3, *right*). We consider here unpolarized incident light, thus $Q = U = V = 0$. For the incoming radiation from (θ_r, ϕ_r), the nonzero elements of the radiation tensor are

$$\bar{J}^0_0 = I_*, \qquad \bar{J}^2_0 = \frac{W_a}{2\sqrt{2}W} (2 - 3 \sin^2\theta_r) I_*, \qquad \bar{J}^2_{\pm 2} = \frac{\sqrt{3} W_a}{4W} \sin^2\theta_r I_* e^{\pm 2i\phi_r}, \qquad \bar{J}^2_{\pm 1} = \mp \frac{\sqrt{3} W_a}{4W} \sin 2\theta_r I_* e^{\pm i\phi_r}, \tag{6}$$

where W is the dilution factor of the radiation field, which can be divided into an anisotropic part W_a and an isotropic part W_i (Bommier & Sahal-Brechot 1978). The solid-angle-averaged intensity for a blackbody radiation source is

$$I_* = W \frac{2h\nu^3}{c^2} \frac{1}{e^{h\nu/k_B T} - 1}. \tag{7}$$

By setting the first terms on the left-hand side of equation (1) to zeros, we can obtain the following linear equations for the steady state density tensors in the ground states of atoms,

$$i\Gamma\rho_q^k(J_l)q - \sum_{J_u,k'}\left\{p_k(J_u,J_l)\frac{[J_u]}{\sum_{J_l''}A''/A+i\Gamma' q}\sum_{J_l'}[J_l']\left[\delta_{kk'}p_{k'}(J_u,J_l')+\sum_{Qq'}r_{kk'}(J_u,J_l,Q,q')\frac{\bar{J}_Q^2}{\bar{J}_0^0}\right]\right.$$
$$\left.-\left[\delta_{kk'}+\sum_{Q,q'}s_{kk'}(J_u,J_l,Q,q')\frac{\bar{J}_Q^2}{\bar{J}_0^0}\right]\right\}\rho_{-q'}^{k'}(J_l)=0, \tag{8}$$

where $\Gamma = 2\pi\nu_{\rm L}g_l/B_{lu}\bar{J}_0^0$ and $\Gamma' = 2\pi\nu_{\rm L}g_u/A$.

The multiplet effect is accounted for by summing over J_u. The alignment of atoms induces polarization for absorption lines. Depending on the comparison between the first term (due to magnetic mixing) and the other terms (due to optical pumping), there could be different regimes. In our previous studies (YL06, YL07), we dealt with the regime where magnetic mixing is the fastest process; this is the regime for atomic realignment (see Fig. 1). When magnetic splitting $2\pi\nu_{\rm L}g_l$ is comparable to the photon pumping rate $B\bar{J}_0^0$, the coherence terms $\rho_{q\neq0}^k$ appear. Physically, this is because magnetic field cannot remain a good quantization axis when the two processes magnetic precession and optical pumping happen on comparable timescales (unless the magnetic field is aligned along the symmetry axis of the radiation field). In such a situation, the density matrix of the ground level becomes sensitive to the strength of the magnetic field. This is the *lower level Hanle regime*. Absorption from the ground level will be polarized, and the polarization gets the imprint of the magnetic field. The corresponding absorption coefficients η_i are (Landi Degl'Innocenti 1984; see also YL06)

$$\eta_i(\nu,\Omega) = \frac{h\nu_0}{4\pi}Bn(J_l)\Psi(\nu-\nu_0)\sum_{KQ}(-1)^K w_{J_lJ_u}^K\sigma_Q^K(J_l)\mathcal{J}_Q^K(i,\Omega), \tag{9}$$

where $n(J_l) = n\sqrt{[J_l]}\rho_0^0(J_l)$ is the total atomic population on level J_l, $\Psi(\nu-\nu_0)$ is the line profile, $\sigma_Q^K \equiv \rho_Q^K/\rho_0^0$, and

$$w_{J_lJ_u}^K \equiv \begin{Bmatrix}1 & 1 & K\\ J_l & J_l & J_u\end{Bmatrix}\Big/\begin{Bmatrix}1 & 1 & 0\\ J_l & J_l & J_u\end{Bmatrix}. \tag{10}$$

The polarization produced by absorption through optical depth $\tau = \eta_0 d$ is

$$\frac{Q}{I\tau} = \frac{-\eta_1 dI_0}{(1-\eta_0 d)I_0\eta_0 d} \simeq -\frac{\eta_1}{\eta_0}, \qquad \frac{U}{I\tau} \simeq -\frac{\eta_2}{\eta_0}. \tag{11}$$

In our choice of reference, only coherence density components contribute to U (see eqs. [9] and [6]). Therefore, unlike the case for atomic realignment U is not zero in the *ground Hanle regime*. Since incoming light is unpolarized, there is no orientation for the atoms. The circular polarization component is thus zero, $V = \epsilon_3 = 0$.

The differential occupation on the ground state (eq. [8]) can be transferred to the upper level of an atom by excitation,

$$\rho_q^k(J_u) = \frac{1}{\sum_{J_l''}A''+iA\Gamma' q}\sum_{J_l'k'}[J_l']\left[\delta_{kk'}p_{k'}(J_u,J_l')B_{lu}\bar{J}_0^0+\sum_{Qq'}r_{kk'}(J_u,J_l',Q,q')B_{lu}\bar{J}_Q^2\right]\rho_{-q'}^{k'}(J_l). \tag{12}$$

Emission from such a differentially populated state is polarized; the corresponding emission coefficients of the Stokes parameters are (Landi Degl'Innocenti 1984)

$$\epsilon_i(\nu,\Omega) = \frac{h\nu_0}{4\pi}An(J_u,\theta_r)\Psi(\nu-\nu_0)\sum_{KQ}w_{J_uJ_l}^K\sigma_Q^K(J_u,\theta_r)\mathcal{J}_Q^K(i,\Omega), \tag{13}$$

where $n(J_u) = n\sqrt{[J_u]}\rho_0^0(J_u)$ is the total population on level J_u. For the optically thin case, the linear polarization degree $p = (Q^2+U^2)^{1/2}/I = (\epsilon_2^2+\epsilon_1^2)^{1/2}/\epsilon_0$ and the positional angle $\chi = \frac{1}{2}\tan^{-1}(U/Q) = \frac{1}{2}\tan^{-1}(\epsilon_2/\epsilon_1)$. Obviously, unlike the case of pure magnetic realignment, in the presence of stronger magnetic fields the positional angle χ experiences variations with the magnetic field strength.

4. POLARIZATION IN MAGNETIC REALIGNMENT REGIME

4.1. *Polarization of Absorption Lines*

In the regime of the weak field, polarization of absorption lines arising from aligned atoms was dealt with for atoms with fine structure in YL06 and with hyperfine structure in YL07. Since that time, we have provided calculations for more atomic lines. In particular, we show below the results for Ti II, which has transitions in the optical band, and those can be observed from the *ground* (see Table 2). The calculations follow the same approach that we discussed in detail in YL06.

TABLE 2
Absorption Lines

Species	Ground State	Excited State	Wavelength (Å)	$P_{\max}$ (%)
Ti II	$a4F_{3/2}$	$z4G^o_{5/2}$	3384.74	−0.7
		$z4F^o_{5/2}$	3230.13	−0.7
		$z4F^o_{3/2}$	3242.93	2.9
		$z4D^o_{3/2}$	3067.25	2.9
		$z4D^o_{1/2}$	3073.88	7.3

The geometry of the radiation system is illustrated by Figure 3 (*left*). The origin of this frame is defined as the location of the atomic cloud. The line of sight defines the z-axis, and together with the direction of radiation, they specify the x-z plane. The x-y plane is thus the plane of sky. In this frame, the incident radiation is coming from $(\theta_0, 0)$, and the magnetic field is in the direction (θ_B, ϕ_B).

The magnetic field is chosen as the quantization axis (z'') for the atoms. In this "theoretical" reference frame, the line of sight is in the (θ, π)-direction (i.e., the x''-z'' plane is defined by the magnetic field and the line of sight; see Fig. 3, *right*), and the radiation source is directed along (θ_r, ϕ_r).

In YL06 we discussed that the resonance absorption lines that are appropriate for studying magnetic fields in diffuse, low–column density (AV ∼few tenths) neutral clouds in the interstellar medium (ISM) are N I, O I, S II, Mn II, and Fe II. These are all in the ultraviolet. At higher column densities, the above lines become optically thick, and lines of lower abundance, as well as excited states of the above lines, become available. Significantly, some of these alignable species, e.g., Ti II and Fe I, are in the visible.

The Ti II lines provide a fairly accessible test of the magnetic alignment diagnostic. Ti II has a metastable state $b4F_{3/2,5/2,7/2,9/2}$ in addition to the ground state $a4F_{3/2,5/2,7/2,9/2}$ and the excited states $z4D^o_{1/2,3/2,5/2}$, $z4F^o_{3/2,5/2,7/2,9/2}$, and $z4G^o_{5/2,7/2,9/2}$. By including all the transitions between the excited and the metastable states, we obtain the alignment of Ti II (Fig. 4). The polarization of the absorption line can then be obtained according to equation (11),

$$\frac{P}{\tau} \simeq -\frac{\eta_1}{\eta_0} = \frac{1.5\sigma_0^2(J_l)\sin^2\theta w^2_{J_l J_u}}{\sqrt{2} + \sigma_0^2(J_l)\left(1 - 1.5\sin^2\theta\right) w^2_{J_l J_u}}. \tag{14}$$

The predictions for the polarization are shown in Figure 4. In addition, the line ratios are also modulated by the alignment (Fig. 5). Table 2 summarizes the list of lines with predictions of the polarization arising from the realignment of Ti II in its ground state.

4.2. *Polarization of Emission Lines of Atoms with Fine Structure*

The magnetic realignment diagnostic can also be used in emission, for resonant or fluorescent scattering lines. The weak field regime for the atoms with fine structure was not covered completely in YL06. While the calculations of the polarization arising from absorption of aligned atoms with fine structure were provided in YL06, there we did not provide the calculations for the emission line polarization arising from such atoms. We, however, proved in YL07 that emission polarization studies may be important for aligned atoms with hyperfine structure. Below we correct the deficiency of our earlier studies and discuss the polarization arising from the emission of atoms with fine structure.

When the magnetic precession rate becomes less than the emission rate of the upper level, the effect of magnetic field on the upper level is negligible. The only influence of magnetic field is on the ground state through the alignment of atoms. The atoms are aligned either parallel or perpendicular to the magnetic field. The photons absorbed or scattered by such aligned atoms are polarized in accordance with the geometrical relation of the magnetic field with respect to the incoming light and line of sight. The detection of the polarizations of the emission and/or absorption thus provide three-dimensional information about the magnetic field. In YL06, we studied the polarizations of

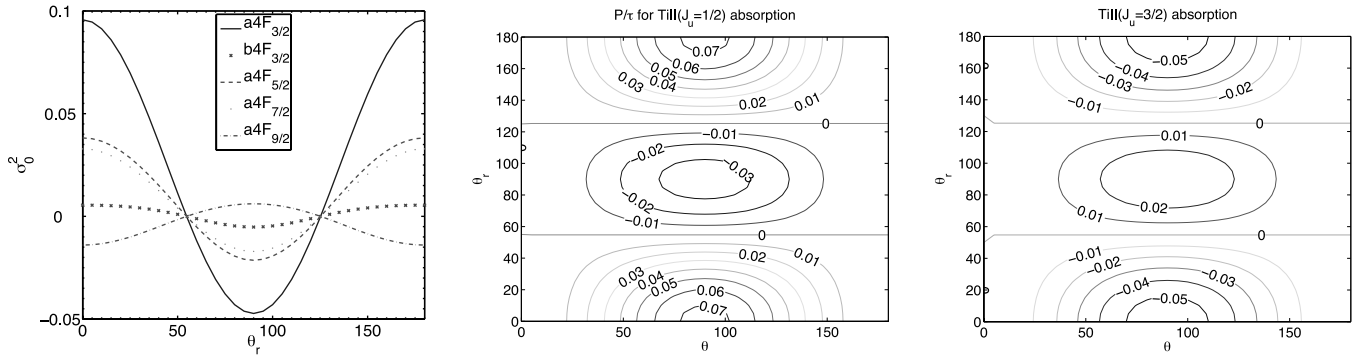

Fig. 4.—*Left*: Alignment of the ground state $a4F$ and metastable level $b4F_{3/2}$ of Ti II. *Middle and right*: Contours of equal degrees of polarization of Ti II absorption lines ($J_l = 1/2 \rightarrow J_u = 1/2, 3/2$). The angles θ_r and θ are the angles of incident radiation and line of sight from the magnetic field (see Fig. 1, *right*). In the case of a pumping source coincident with the background source, we have that the degeneracy and polarization will be determined by one parameter $\theta_r = \theta$. [*See the electronic edition of the Journal for a color version of this figure.*]

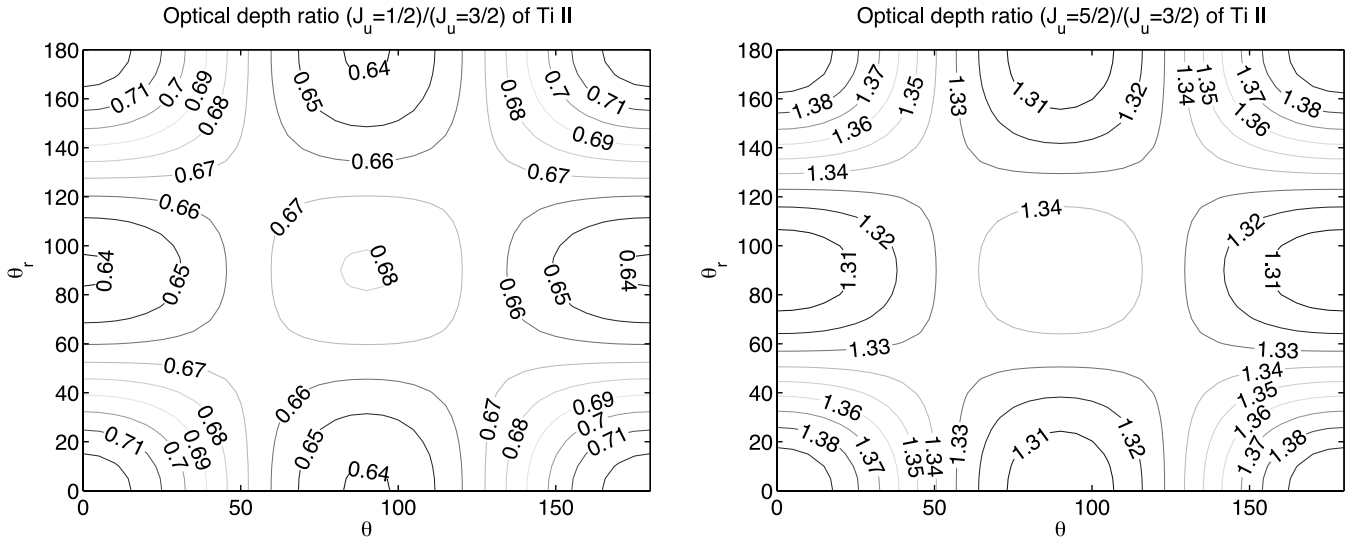

FIG. 5.— Variations of the Ti II line ratios caused by the atomic alignment. [*See the electronic edition of the Journal for a color version of this figure.*]

absorption lines arising from the atomic alignment. Here we shall use a couple of examples (S II and O I, see Table 3 and Fig. 6) to illustrate the emission line polarimetry induced by the atomic alignment.

To remind our readers, S II has a ground level $4S^o_{3/2}$ and upper levels $4P_{1/2,3/2,5/2}$, which means $J_l = 3/2$ and $J_u = 1/2, 3/2$, and 5/2. The irreducible density tensor of the ground state $\rho^k_q(J_l)$ has components with $k = 3/2 - 3/2, 3/2 - 1/2, \ldots, 3/2 + 3/2 = 0, 1, 2, 3$. The ground state alignment we obtained in YL06 for S II is

$$\sigma^2_0(J_l) = \frac{1.0481 - 3.1442\cos^2\theta_r}{0.264\cos^2\theta_r - 13.161}. \tag{15}$$

The basic formalism is described in § 3 (eqs. [1]–[8] and [12]–[13]) except that we are now in a limiting case $\Gamma' \to 0$ and $\Gamma \gg 1$. By inserting equation (15) into equation (12), we obtain

$$\rho^0_0\begin{pmatrix} J_u = 3/2 \\ J_u = 5/2 \end{pmatrix} = \frac{BI_*}{A}\rho^0_0(J_l)\begin{pmatrix} 1.887\cos^4\theta_r - 0.886\cos^2\theta_r - 12.987 \\ 1.6634\cos^4\theta_r + 6.1058\cos^2\theta_r - 2.220 \end{pmatrix}\Big/\left(1.487\cos^2\theta_r - 52.787\right),$$

$$\rho^2_0\begin{pmatrix} J_u = 3/2 \\ J_u = 5/2 \end{pmatrix} = \frac{BI_*}{A}\rho^0_0(J_l)\begin{pmatrix} -0.385\cos^4\theta_r + 0.560\cos^2\theta_r - 10.818 \\ -0.2413\cos^4\theta_r - 7.7510\cos^2\theta_r + 2.6105 \end{pmatrix}\Big/\left(1.487\cos^2\theta_r - 52.787\right),$$

$$\rho^2_2\begin{pmatrix} J_u = 3/2 \\ J_u = 5/2 \end{pmatrix} = \frac{BI_*}{A}\rho^0_0(J_l)e^{-2i\phi_r}\sin^2\theta_r\begin{pmatrix} 3.4892 - 0.86125\cos^2\theta_r \\ 0.23763\cos^2\theta_r - 2.5249 \end{pmatrix}\Big/\left[(1.487 + 2.975i\Gamma')\cos^2\theta_r - 52.787 - 105.57i\Gamma'\right],$$

$$\rho^2_1\begin{pmatrix} J_u = 3/2 \\ J_u = 5/2 \end{pmatrix} = \frac{BI_*}{A}\rho^0_0(J_l)e^{-i\phi_r}\sin 2\theta_r\begin{pmatrix} -0.2940\cos^2\theta_r - 3.1041 \\ 0.0145\cos^2\theta_r + 2.4409 \end{pmatrix}\Big/\left[\left(1.487\cos^2\theta_r - 52.787\right)(1 + i\Gamma')\right]. \tag{16}$$

TABLE 3
EMISSION LINES

Species	Lower State	Upper State	Wavelength (Å)	$\lvert P_{\max}\rvert$ (%)
S II	$4S^o_{3/2}$	$4P_{3/2}$	1253.81	30.6
		$4P_{5/2}$	1259.52	31.4
O I	$3P_0$	$3S^o$	1306	16
	$3P_1$	$3S^o$	1304	8.5
	$3P_2$	$3S^o$	1302	1.7
	$3P$	$3S^o$	5555, 6046, 7254	2.3
	$3P_0$	$3D^o$	1028	4.29
	$3P_1$	$3D^o$	1027	7.7
	$3P_2$	$3D^o$	1025	10.6
	$3P$	$3D^o$	5513, 5958, 7002	1.3

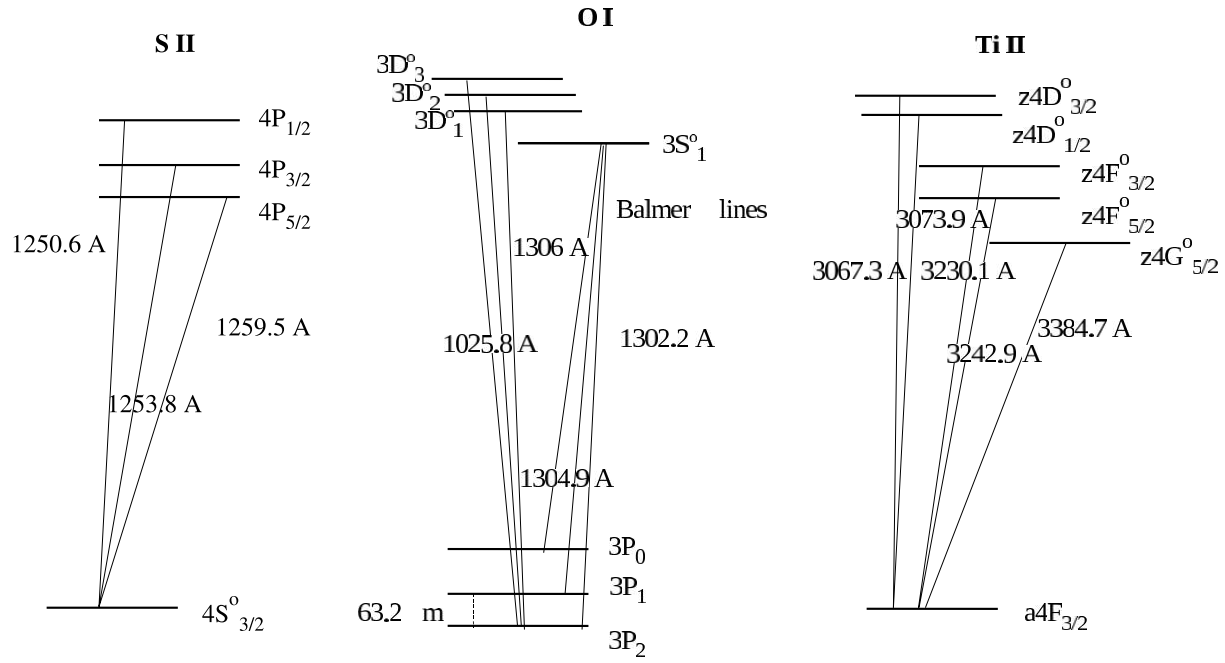

FIG. 6.—*Left*: Schematics of the transitions within the fine structure of S II. *Middle*: Same as the left panel, but for O I. *Right*: Same as the left panel, but for Ti II.

In the magnetic realignment regime, we can directly get the density matrices by setting $\Gamma' = 0$ in the equation. Then for the optically thin case, the Stokes parameters can be readily obtained by inserting the density matrices into equation (13). The results in the optically thin case $Q/I \simeq \epsilon_1/\epsilon_0$, $U/I \simeq \epsilon_2/\epsilon_0$ are illustrated in Figure 7 and Table 3.

Another atomic species, namely, O I, can be used as a magnetic field diagnostic. It can be used, for instance, in reflection nebulae, since the lack of ionizing flux limits the number of levels being pumped and especially since it is common that the atom is not ionized, which eliminates the interference of the recombination radiation. The fluorescent line O I λ8446 can be seen in spectra by Gordon et al. (2000) in NGC 7023.

We attained the density matrices of the ground state in YL06. The density matrices on the upper level occupation are then obtained by inserting them into equation (12),

$$\rho_0^0(J_u) = \frac{\rho_0^0(J_l)[J_l]B}{\sum A''}\left[p_0(J_u,J_l)\bar{J}_0^0 + r_{02}(J_u,J_l)\bar{J}_0^2\sigma_0^2(J_l)\right],$$

$$\rho_0^2(J_u) = \frac{\rho_0^0(J_l)[J_l]B}{\sum A''}\left\{\left[p_2(J_u,J_l)\bar{J}_0^0 + r_{22}(J_u,J_l,0,0)\bar{J}_0^2\right]\sigma_0^2(J_l) + \left[r_{20}(J_u,J_l,0,0) + r_{24}(J_u,J_l,0,0)\sigma_0^4(J_l)\right]\bar{J}_0^2\right\},$$

$$\rho_{\pm2}^2(J_u) = \frac{\rho_0^0(J_l)[J_l]B}{\sum A'' \pm i2A\Gamma'}\left[r_{20}(J_u,J_l,-2,2) + \sigma_0^2(J_l)r_{22}(J_u,J_l,-2,2) + r_{24}(J_u,J_l,-2,2)\sigma_0^4(J_l)\right]\bar{J}_{\mp2}^2,$$

$$\rho_{\pm1}^2(J_u) = \frac{\rho_0^0(J_l)[J_l]B}{\sum A'' \pm iA\Gamma'}\left[r_{20}(J_u,J_l,-1,1) + \sigma_0^2(J_l)r_{22}(J_u,J_l,-1,1) + r_{24}(J_u,J_l,-1,1)\sigma_0^4(J_l)\right]\bar{J}_{\mp1}^2, \quad (17)$$

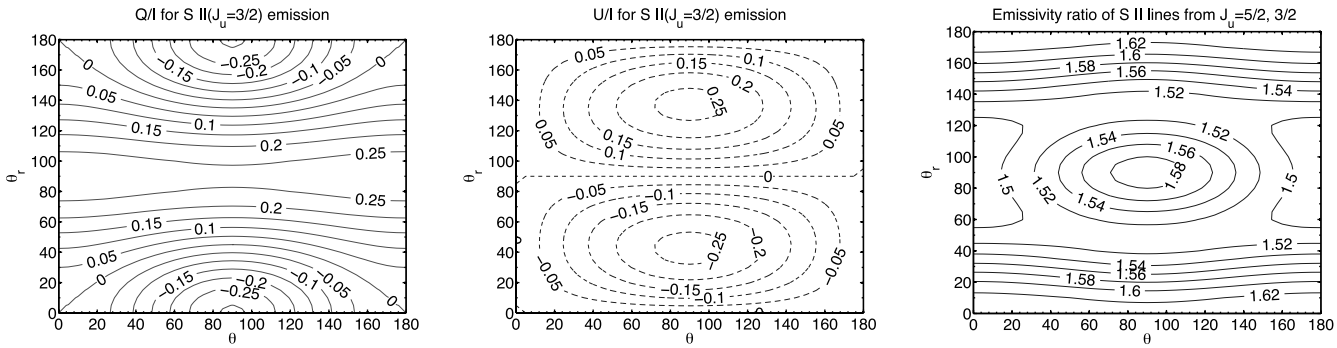

FIG. 7.—*Left and middle*: Contour graphs of S II emission line polarization from $J_u = 5/2$. *Right*: Contour graph of the emissivity ratio of lines from $4P_{5/2,3/2}$ to $4S^o$. We adopted the parameters $R_{SD} = 2.36$ (eq. [19]) and $\phi_r = \pi/2$ (see Fig. 3, *right*). [*See the electronic edition of the Journal for a color version of this figure.*]

where

$$\begin{bmatrix}\sigma_0^2(J_l)\\ \sigma_0^4(J_l)\end{bmatrix}=\begin{bmatrix}\dfrac{\left(5.135+13.183R_{SD}-44.666R_{SD}^2\right)\cos^4\theta_r+\left(-46.389+31.12R_{SD}+113.15R_{SD}^2\right)\cos^2\theta_r+14.892-32.755R_{SD}^2-11.838R_{SD}}{\left(-2.35-5.654R_{SD}+11.837R_{SD}^2\right)\cos^4\theta_r+\left(21.789+47.27R_{SD}+37.903R_{SD}^2\right)\cos^2\theta_r-71.847-133.38R_{SD}^2-199.188R_{SD}}\\ \dfrac{\left(1-2.976R_{SD}+2.017R_{SD}^2\right)\left(-11.885\cos^4\theta_r+7.923\cos^2\theta_r-1.321\right)}{\left(-2.35-5.654R_{SD}+11.837R_{SD}^2\right)\cos^4\theta_r+\left(21.789+47.27R_{SD}+37.903R_{SD}^2\right)\cos^2\theta_r-71.847-133.38R_{SD}^2-199.188R_{SD}}\end{bmatrix}, \tag{18}$$

$$R_{SD}=\sum_{S21} I_\nu S_\nu \Big/ \sum_{D23} I_\nu S_\nu \tag{19}$$

is a measure of the ratio of transitional probabilities from $^3P_2$ to $^3S_1^o$ states and $^3D_3^o$ states (see also YL06), where the line strength S_ν can be found, e.g., in the NIST Atomic Spectra Database.[4] We emphasize that there are actually many states of different energies for the $^3S^o$ term and $^3D^o$ term. All of the transitions should be taken into account when calculating R_{SD}. Inserting equations (6) and (17) and $w^2_{J_uJ_l}$ (eq. [10], see also Table 4 in YL06) into equation (13), using the coefficients given in Table 4, we get the polarization of the emission lines (see Table 3). Figure 8 shows the polarization of lines $^3S^o \rightarrow {}^3P_1$ for weak pumping[5] in the case of $R_{SD} \simeq 2.36$. Note that lines with the same initial and final terms have the same polarization regardless of their energy state. This is because it is the angular momentum that is the key quantity for the atomic alignment process. Therefore, many optical lines (see Grandi 1975) arising from transitions at the higher excited states can be easily inferred from the transitions to the ground state (see Table 3). From equation (17), we see that the density tensors $\rho_q^2(J_u)$ have finite values even if the atomic alignment $(\sigma^2, 4_0)$ is completely neglected. Indeed, the polarization of scattering lines are frequently discussed in the literature without accounting for what happens on the ground state (see, e.g., Stenflo 1994). This oversimplified approach, however, brings erroneous results as we show here. Table 4 lists the numerical coefficients needed for the calculations of the alignment of the three species Ti II, O I, and S II.

5. POLARIZATION IN HANLE REGIME

In what follows, we shall use S II as an example to discuss the aforementioned different polarization regimes. S II absorption lines are observed in the ISM (Morton 1975). Since we have discussed the polarization of S II in the atomic alignment regime, having the same species studied in different regimes enables us to better understand how the atomic polarization changes with the magnetic field strength and the environment.

5.1. *Upper Level Hanle Regime*

The Hanle effect has been known since the 1920s and directly associated with the coherence of pure atomic states (see Bohr 1924; Hanle 1924; Heisenberg 1925). Observationally, it is rotation and depolarization of resonant scattered light in a weak magnetic field compared to the nonmagnetized case. Although semiclassical theory can give us a qualitative picture, generic theory based on quantum electrodynamics (QED) and the density matrix has to be invoked to give an accurate description (see Landi Degl'Innocenti 1999; Trujillo Bueno 1999).

One of the major changes introduced by the QED approach is the ability to include atomic polarization on the ground level. This effect was ignored in most cases for a long time, although a few exceptions can be found (Bommier 1977; Landi Degl'Innocenti 1982). Although the Hanle effect has been noticed and applied to stellar winds, the effect of ground level polarization, however, was still excluded (see, e.g., Ignace et al. 1999).

In the Hanle regime, the influence of magnetic field on the ground state is exactly the same as in the atomic alignment regime. So the polarization of the absorptions has the same pattern, namely, either parallel or perpendicular to the magnetic field in the plane of sky. The emission, however, is different. This is because the upper state is also influenced by the magnetic field directly, unlike in the atomic alignment regime. Since the magnetic splitting is comparable to the line width, the density tensors of the upper level are affected by the strength of the magnetic field as well, and they are determined by equation (16).

The dependence of the density tensor components of the upper level $J_u = 5/2$ are shown in the left panel of Figure 9. Inserting these density matrix components into equation (13), one can easily obtain the Stokes parameters in the optically thin case. For the 90° scattering ($\theta_0 = 90^\circ,\ \phi_B = 90^\circ$ or $\theta_r = 90^\circ,\ \phi_r = 270^\circ$ as shown in Fig. 3), the polarization diagrams are shown in Figure 10. For comparison, we also show the density tensors and the Hanle diagrams without ground state alignment ($\sigma_0^2(J_l) = 0$) in Figures 9 and 10. There is a notable difference between them, indicating ground state alignment plays an important role and should be accounted for. In addition to increasing the polarization, the main effect of ground state alignment is to reduce the degeneracy of θ (the angle between the line of sight and magnetic field) when $\Gamma < 1$. In other words, the atomic alignment carries additional information about the direction of magnetic field, which would be veiled otherwise. In the opposite limit, when $\Gamma \gg 1$, the upper state is realigned by the fast magnetic mixing. Similar to the "magnetic realignment regime," $U \rightarrow 0$ in this case and the polarization is either parallel or perpendicular to the magnetic field. This can be important for studies of magnetic fields in the intermediate range ($10\ \mathrm{G} < B \lesssim 100\ \mathrm{G}$).

5.2. *Lower Level Hanle Regime*

If magnetic splitting is comparable to the optical pumping rate, which is the inverse of lifetime in the ground state, an analogy can be made between the ground state in this situation and the upper level in the Hanle regime. In this case, coherence appears and the ground state density matrix is modulated according to the strength and direction of the magnetic field. By solving equation (8), we obtain the following density matrix components for the ground state,

[4] Available at http://physics.nist.gov/PhysRefData/ASD/index.html.
[5] Weak pumping means only pumping from the ground level is considered (see YL06).

TABLE 4

NUMERICAL COEFFICIENTS FOR COMPUTING THE DENSITY MATRICES

$J_i \rightarrow J_f$	p_2	r_{02}	r_{20} $(q = 0, \pm 2)$	r_{20} $(q = \pm 1)$	r_{22} $(q = 0)$	r_{22} $(q = \pm 2)$	r_{22} $(q = \pm 1)$	r_{24} $(q = 0)$	r_{24} $(q = \pm 2)$	r_{24} $(q = \pm 1)$	$s_{02}(s_{20})$	s_{22}	$s_{24}(s_{42})$
$2 \rightarrow 1$	0.15275	0.15275	0.02582	−0.02582	0.0309	−0.0309	−0.0154	0.24842	0.0414	0.1656	0.5916	0.1515	0.2711
$2 \rightarrow 2$	0.1	−0.11832	−0.11832	0.11832	−0.10102	0.1010	0.0505	−5.4210E−2	−0.0090	−0.0361	−0.5916	−0.1515	−0.2711
$2 \rightarrow 3$	0.14	2.8571E−2	0.0828	−0.0828	2.8278E−2	−0.0283	−0.0141	6.3232E−3	0.0011	0.0042	0.169	4.329E−2	7.7444E−2
$3/2 \rightarrow 1/2$	0	0.25	0	0	0	0	0	NA	NA	NA	0.28284	0	0
$3/2 \rightarrow 3/2$	0.05	−0.14142	−0.14142	0.14142	−0.14142	0.14142	0.0707	NA	NA	NA	−0.22627	0	0
$3/2 \rightarrow 5/2$	1.5275E−1	2.8868E−2	0.10801	−0.10801	3.0861E−2	−3.0861E−2	−1.543E−2	NA	NA	NA	5.657E−2	0	0

NOTE.—The values in the first and second rows are for O I, and the values in the third through the fifth rows are for Ti II and S II (see eqs. [1]–[3]).

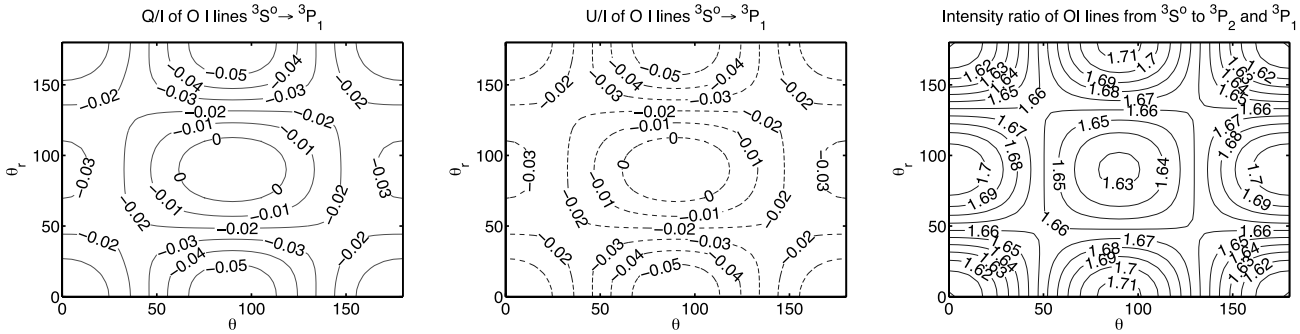

FIG. 8.—*Left and middle*: Contour graphs of polarization of O I lines $^3S^o \rightarrow {}^3P_1$. *Right*: Contour graph of the emissivity ratio of O I lines from $^3S^o$ to $^3P_{2,1}$, with $\phi_r = \pi/2$. We consider here the weak pumping regime, where only pumping from the ground level is accounted for (YL06). [*See the electronic edition of the Journal for a color version of this figure*.]

$$\begin{aligned}\rho_0^2/\varrho_0^0 =& -10825-(31990\cos 2\theta_r+10663)\Gamma^4-\cos 6\phi_r\Gamma^2+2\cos 6\phi_r\cos 2\theta_r\Gamma^2-79494\cos 2\theta_r\Gamma^2-\cos 6\phi_r\\ &\times\cos 4\theta_r\Gamma^2+397\cos 4\theta_r\Gamma^2-26393\Gamma^2-428\left(-0.5\Gamma^2+\left(\Gamma^2+0.5\right)\cos 2\theta_r+\left(-0.5\Gamma^2-0.25\right)\cos 4\theta_r\right)\\ &\times\sin 2\phi_r\Gamma-107\left(-0.75\Gamma^2+\left(\Gamma^2+2\right)\cos 2\theta_r-\left(0.25\Gamma^2+0.54\right)\cos 4\theta_r+0.02\cos 6\theta_r-1.47\right)-\sin 4\phi_r\Gamma\\ &-4.3(\cos 2\theta_r-0.4\cos 4\theta_r-0.66)\sin 6\phi_r\Gamma+\cos 6\phi_r-2\cos 6\phi_r\cos 2\theta_r-32222\cos 2\theta_r+\cos 6\phi_r\cos 4\theta_r\\ &-113\cos 4\theta_r-\cos 6\theta_r+\cos 4\phi_r\left[-\cos 6\theta_r\Gamma^2+55\Gamma^2-\left(74\Gamma^2+151\right)\cos 2\theta_r+\left(20\Gamma^2+38\right)\cos 4\theta_r+113\right]\\ &+\cos 2\phi_r\left[3\Gamma^2+\left(-607\Gamma^2-306\right)\cos 2\theta_r+\left(607\Gamma^2+306\right)\cos 4\theta_r-3(\Gamma^2-0.95^2)\cos 6\theta_r\right],\end{aligned}$$

$$\begin{aligned}\Re\left(\rho_2^2\right)/\varrho_0^0 =& 369\Gamma^2\cos 4\phi_r\sin^4\theta_r-374\cos 4\phi_r\sin^4\theta_r-8\Gamma^2\cos 4\phi_r\cos 2\theta_r\sin^4\theta_r-760\Gamma\sin 4\phi_r\sin^4\theta_r\\ &+39\Gamma\cos 2\theta_r\sin 4\phi_r\sin^4\theta_r-12215\Gamma^2\cos 2\phi_r\sin^2\theta_r-26433\cos 2\phi_r\sin^2\theta_r+922\Gamma^2\cos 2\phi_r\cos 2\theta_r\sin^2\theta_r\\ &+3\cos 2\phi_r\sin^2\theta_r(\cos 2\theta_r-\cos 4\theta_r)+\left[(524\cos 2\theta_r-18264)\Gamma^2-34687+3112\cos 2\theta_r-15\cos 4\theta_r\right]\\ &\times\Gamma\sin 2\phi_r\sin^2\theta_r-140\Gamma^2+188\Gamma^2\cos 2\theta_r-48\cos 4\theta_r(\Gamma^2+1)+186\cos 2\theta_r-139,\end{aligned}\tag{20}$$

$$\begin{aligned}\Im\left(\rho_2^2\right)/\varrho_0^0 =& (9263\cos 2\phi_r+131\cos 2\phi_r\cos 4\theta_r-9394\cos 2\phi_r\cos 2\theta_r)\Gamma^3-6707\sin 2\phi_r\Gamma^2+140\sin 4\phi_r\Gamma^2+139\sin 2\phi_r\cos 4\theta_r\Gamma^2\\ &-188\sin 4\phi_r\cos 2\theta_r\Gamma^2+6570\sin 2\phi_r\cos 2\theta_r\Gamma^2+48\sin 4\phi_r\cos 4\theta_r\Gamma^2-\sin 2\phi_r\cos 6\theta_r\Gamma^2+18903\cos 2\phi_r\Gamma\\ &+298\cos 4\phi_r\Gamma-\cos 4\phi_r\cos 6\theta_r\Gamma-\cos 2\phi_r\cos 6\theta_r\Gamma-399\cos 4\phi_r\cos 2\theta_r\Gamma+101\cos 4\phi_r\cos 4\theta_r\Gamma-134\cos 2\theta_r\Gamma\\ &+36\cos 4\theta_r\Gamma-\cos 6\theta_r\Gamma-18905\cos 2\phi_r\cos 2\theta_r\Gamma+3\cos 2\phi_r\cos 4\theta_r\Gamma+99\Gamma-12848\sin 2\phi_r-138\sin 4\phi_r\\ &+\sin 4\phi_r\cos 6\theta_r+\sin 2\phi_r\cos 6\theta_r-371\sin 2\phi_r\cos 4\theta_r+186\sin 4\phi_r\cos 2\theta_r-49\sin 4\phi_r\cos 4\theta_r+13219\sin 2\phi_r\cos 2\theta_r,\end{aligned}$$

$$\begin{aligned}\frac{\Re(\rho_1^2)}{\varrho_0^0} =& \left\{\Gamma\left[-45\sin 2\phi_r\left(\cos^2\theta_r-18\right)\sin^2\theta_r-7.5\sin 4\phi_r\left(\cos^2\theta_r-1\right)^2\right]\cos\phi_r+\left[(\sin^2\phi_r\cos^4\theta_r-\sin^2\phi_r\cos^2\theta_r\right.\right.\\ &+5\cos 2\theta_r-\cos 4\theta_r-4)\cos^2 2\phi_r+(21\Gamma^2\sin^2\phi_r\sin^4\theta_r+185\Gamma^2-183\Gamma^2\cos 2\theta_r-\Gamma^2\cos 4\theta_r+738\sin^2\theta_r)\\ &\times\cos 2\phi_r+51821\Gamma^2-369\Gamma^2\sin^2\phi_r+3\Gamma^2\cos 4\theta_r\sin^2\phi_r-738\sin^2\phi_r+\Gamma^2\cos 4\theta_r+\cos 4\theta_r+\cos 2\theta_r\\ &\times\left(-737\Gamma^2+\left(367\Gamma^2+738\right)\sin^2\phi_r+365\right)+26064\left.\left.\right]\cos\phi_r+\Gamma\left[-6980\Gamma^2+\left(262\Gamma^2-396\right)\cos 2\theta_r+\cos^2 2\phi_r\right.\right.\\ &\left.\left.\times(-4\cos 2\theta_r+\cos 4\theta_r+23)+5\cos 4\theta_r+\cos 2\phi_r(-400\cos 2\theta_r+6\cos 4\theta_r+394)-18507\right]\sin\phi_r\right\}\sin 2\theta_r,\end{aligned}$$

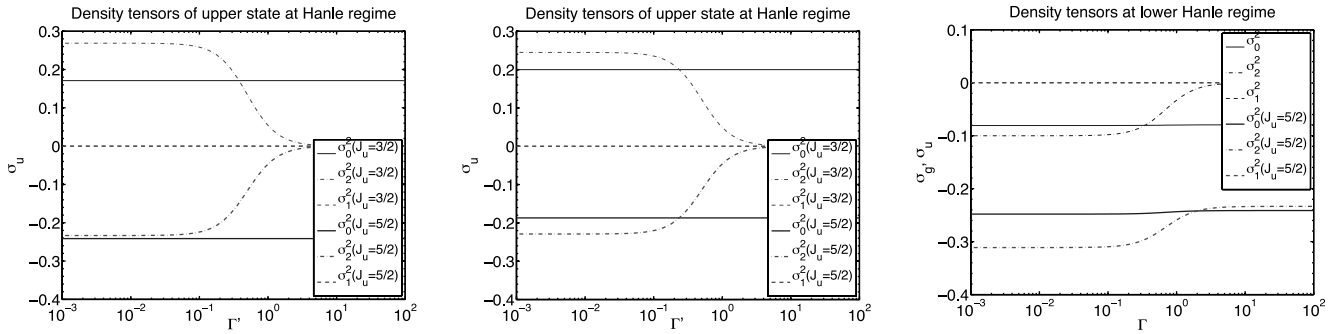

FIG. 9.—Density matrix components vs. the ratio of magnetic splitting to the inverse of the lifetime of a level for 90° scattering. Magnetic field is perpendicular to the radiation field, $\phi_B = 90°$. *Left*: Density components of upper states vs. $\Gamma' = 2\pi\nu_L g_u/A$ in the Hanle regime. As we see, coherence components σ_2^2 are reduced with the increase of the magnetic field strength. In the limit of $\Gamma' \gg 1$, the coherence disappears, corresponding to the saturated Hanle regime. *Middle*: Density components of upper states without accounting for ground level alignment in the Hanle regime. *Right*: Density components of upper and ground states vs. $\Gamma = 2\pi\nu_L g_l/B(3/2 \rightarrow 5/2)\bar{J}_0^0$ in the lower level Hanle regime. For $\Gamma \gg 1$, the coherence components become zeros on the ground state, approaching the atomic alignment regime (see YL06, YL07). [*See the electronic edition of the Journal for a color version of this figure*.]

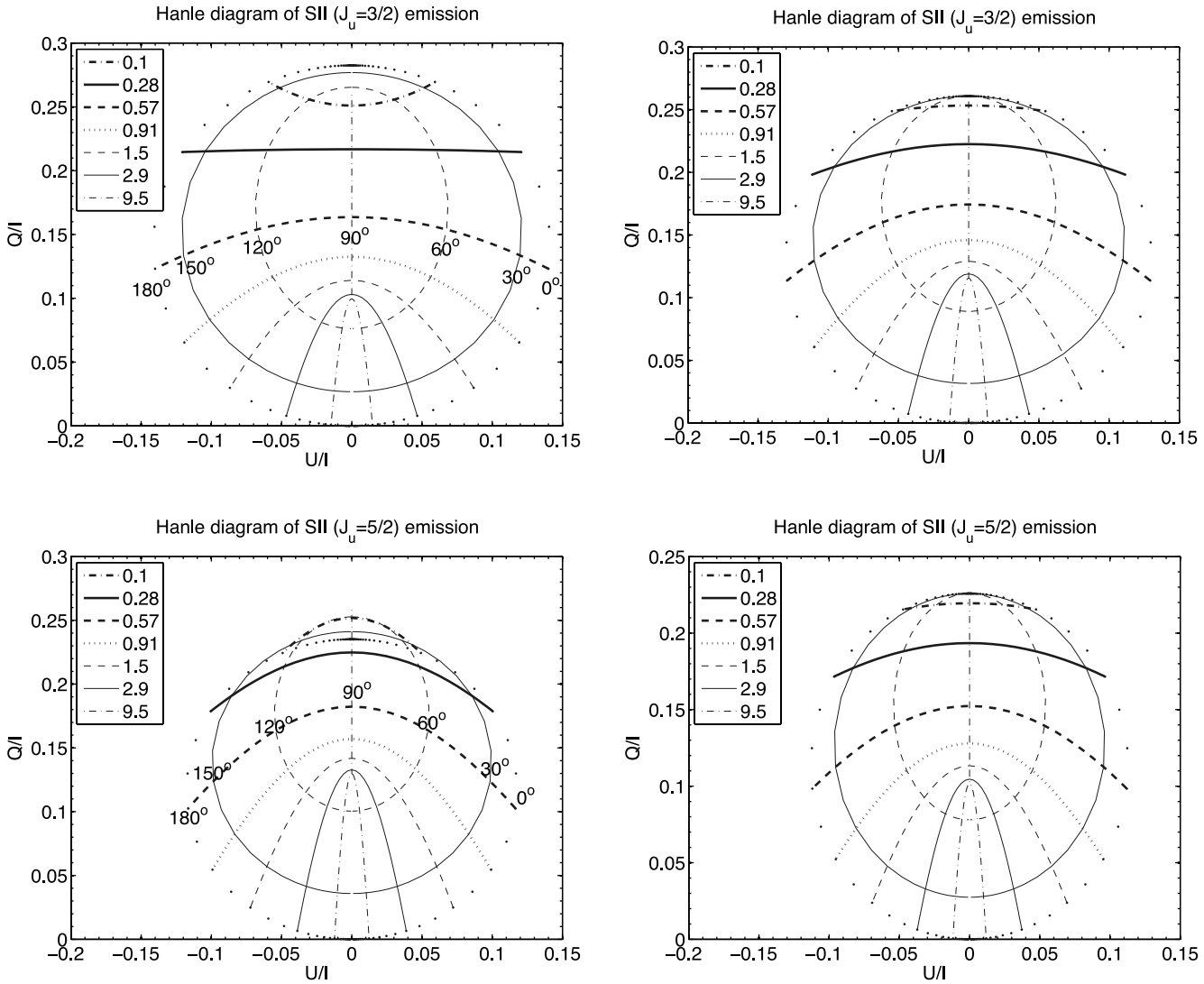

FIG. 10.—Polarization diagram of S II emission lines in the Hanle regime (*left*) and in the Hanle regime, but without accounting for atomic alignment on the ground state (*right*). As in Fig. 9, we have $\theta_0 = 90^\circ$ and $\phi_B = 90^\circ$. The corresponding values of θ are marked in the plots, and the relative strengths of the magnetic field $\Gamma = 2\pi\nu_L g_u/A$ are illustrated in the legend. As $A \simeq 4.4 \times 10^7\ \mathrm{s}^{-1}$, unity in the legend corresponds to a magnetic field of 0.25–25 G. [*See the electronic edition of the Journal for a color version of this figure.*]

$$\Im\left(\rho_1^2\right)/\varrho_0^0 = \big[(473\cos 2\theta_r \sin\phi_r - \cos 4\theta_r \sin\phi_r - 52085\sin\phi_r + 295\cos 2\theta_r \sin 3\phi_r - 4\cos 4\theta_r \sin 3\phi_r - 820\sin 3\phi_r - \cos 2\theta_r \sin 5\phi_r + \sin 5\phi_r)\Gamma^2 - \cos 5\phi_r \Gamma + \cos 5\phi_r \cos 2\theta_r \Gamma + \cos 3\phi_r (397\cos 2\theta_r - 5\cos 4\theta_r - 392)\Gamma + \cos\phi_r(-36790\Gamma^2 + \left(262\Gamma^2 - 390\right)\cos 2\theta_r + 3\cos 4\theta_r - 18511)\Gamma - 373\cos 2\theta_r \sin\phi_r + \cos 4\theta_r \sin\phi_r - 26058\sin\phi_r - 4\cos 2\theta_r \sin 3\phi_r + 4\cos 4\theta_r \sin 3\phi_r - \cos 2\theta_r \sin 5\phi_r + \sin 5\phi_r\big]\sin 2\theta_r,$$

and

$$\rho_{-1}^2 = -\left(\rho_1^2\right)^*, \qquad \rho_{-2}^2 = \left(\rho_2^2\right)^*. \tag{21}$$

In equation (20),

$$\varrho_0^0 = \rho_0^0/\big[(3783\cos 2\theta_r - 264748)\Gamma^4 - (5360\sin 2\phi_r - 5392\cos 2\theta_r \sin 2\phi_r + 31.5\cos 4\theta_r \sin 2\phi_r + 13\cos 2\theta_r \sin 4\phi_r - 3\cos 4\theta_r \sin 4\phi_r - 9\sin 4\phi_r)\Gamma^3 + (13140\cos 2\theta_r - 20\cos 4\theta_r)\Gamma^2 - 658546 - 5317/2\sin 2\phi_r \Gamma + 5271/2\cos 2\theta_r \sin 2\phi_r \Gamma + 23\cos 4\theta_r \sin 2\phi_r \Gamma - 25\cos 2\theta_r \sin 4\phi_r \Gamma + 6\cos 4\theta_r \sin 4\phi_r \Gamma + 19\sin 4\phi_r \Gamma + 52\cos 2\theta_r - 13\cos 4\theta_r + \cos 4\phi_r(7\Gamma^2 + \left(-9\Gamma^2 - 18\right)\cos 2\theta_r + \left(2\Gamma^2 + 5\right) \times \cos 4\theta_r + 13) + \cos 2\phi_r\left(-7558\Gamma^2 + \left(7647\Gamma^2 + 3738\right)\cos 2\theta_r + \left(-89\Gamma^2 + 9\right)\cos 4\theta_r - 3747\right) - 264112\big], \tag{22}$$

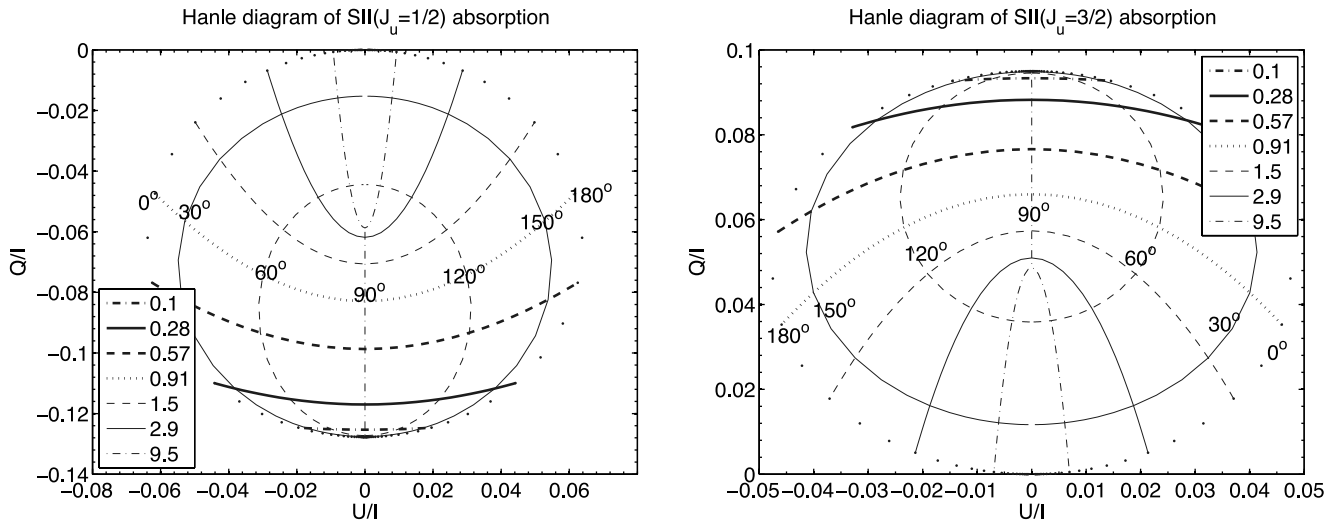

FIG. 11.—Polarization diagram of S II absorption lines in the lower Hanle regime. As in Fig. 9, we have $\theta_0 = 90^\circ$ and $\phi_B = 90^\circ$. The corresponding values of θ are marked in the plots, and the relative strengths of the magnetic field $\Gamma = 2\pi\nu_L g_u/B(3/2 \rightarrow 5/2)\bar{J}_0^0$ are given in the legend. [*See the electronic edition of the Journal for a color version of this figure.*]

where $\rho_0^{0,2}(\Gamma^4)$ is of higher order of Γ compared to other coherent components. Therefore, in the limit $\Gamma \rightarrow \infty$,

$$\sigma_{q\neq 0}^2 = \frac{\rho_{q\neq 0}^2}{\rho_0^2} = 0, \qquad \sigma_0^2 = \frac{\rho_0^2}{\rho_0^2} = -\frac{31{,}990 + 10{,}663\cos 2\theta_r}{264{,}748 - 3783\cos 2\theta_r}, \tag{23}$$

agreeing with our earlier result in the atomic alignment regime (see eq. [17] in YL06). Since the coherent components of the density matrix are not zeros, absorptions in the ground Hanle regime are different from the realignment case.[6] Although the amplitude of the polarization of the absorption lines are comparable (see our Fig. 11 and Fig. 8 in YL06), the direction of polarization becomes a complex function of both the strength and direction of the magnetic field, as there are both Q and U components. It is similar to emission in this sense. Figure 11 is the Hanle diagram of S II absorption for the 90° scattering ($\theta_0 = 90^\circ$, $\phi_B = 90^\circ$; see Fig. 3, *left*). For other geometries, the result can be readily obtained by inserting the density components (eqs. [20]–[22]) into equation (9).

Apparently, the absorption from any lower level including the metastable level would be affected in the same way as long as the absorption rate is comparable to the magnetic precession rate. For instance, the absorptions from the metastable level $b4F$ of Ti II we discussed in § 4.1 and the metastable level $a6D$ of Cr II we studied in YL06 are polarized in the same fashion as S II when $\nu_L \sim \tau_R^{-1}$.

The upper level density matrix is modulated by the magnetic field through excitation from the ground state (see Fig. 9). The analytical expressions of the density matrix of the upper level are extremely lengthy and we do not present them here. They can be attained by inserting equations (20)–(22) into equation (12). Then using equation (13), one can get the polarization of emissions, which also varies with the magnetic field. Figure 12 shows the corresponding Hanle diagram for the 90° scattering. Compared to the Hanle regime, the

[6] Let us remind our reader, in the atomic alignment regime, $U \equiv 0$; thus, polarization can only be parallel or perpendicular to the magnetic field in the plane of sky, and the switch between the two directions always happens at Van Vleck angle $\theta_r = 54.7^\circ$.

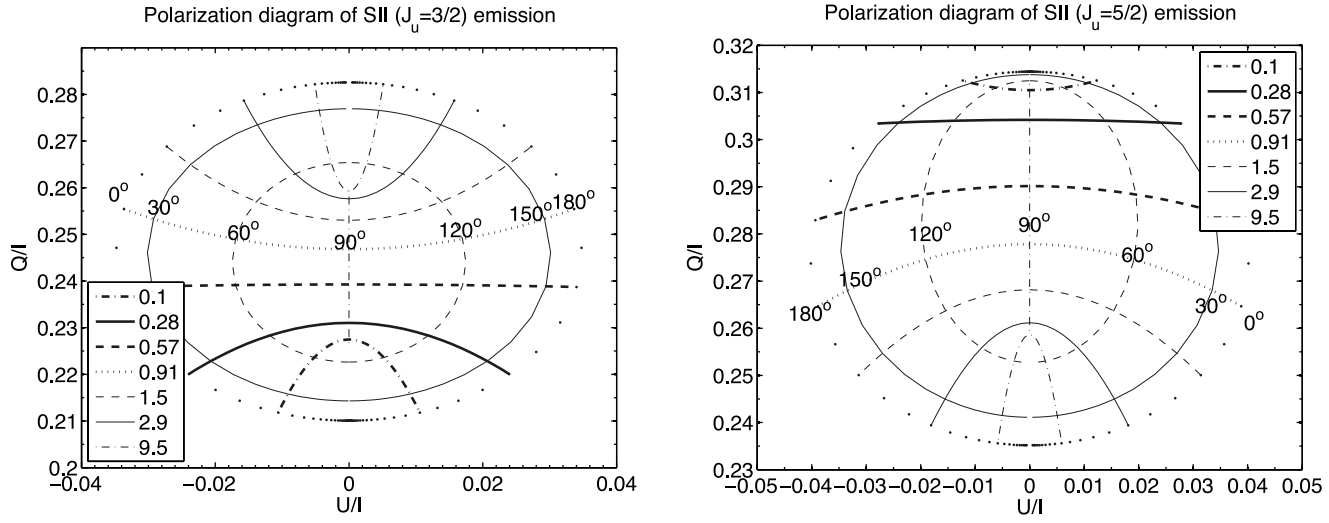

FIG. 12.—Polarization diagram of S II emission lines at the lower Hanle regime. As in Figs. 9 and 11, we have $\theta_0 = 90^\circ$ and $\phi_B = 90^\circ$. [*See the electronic edition of the Journal for a color version of this figure.*]

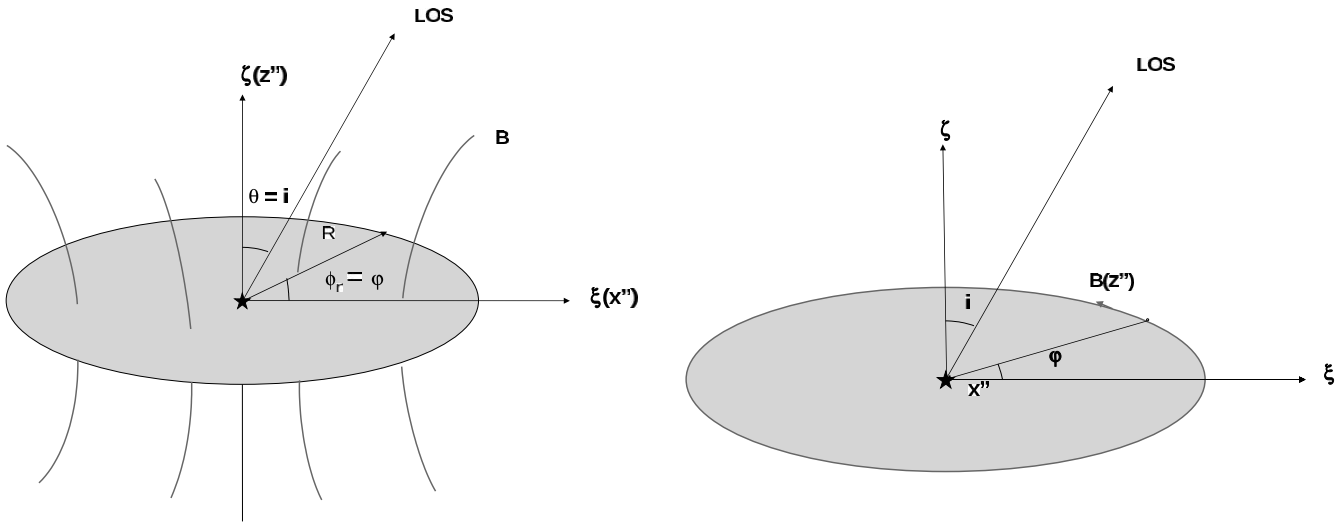

FIG. 13.— Schematic view of a disk with poloidal and toroidal magnetic field. *Left*: In the case of poloidal field, the field lines are normal to the equatorial plane. *Right*: In the case of toroidal field, the field is tangential. In both cases, the radiation from the central source is normal to the field lines. [*See the electronic edition of the Journal for a color version of this figure.*]

polarizations in the ground Hanle regime are larger. This is expected as the magnetic field in the ground Hanle regime is much weaker than that in the Hanle regime (see Fig. 1). Therefore, the depolarization caused by magnetic precession is smaller.

A quantitative comparison can be made with earlier studies (e.g., Landolfi & Landi Degl'Innocenti 1986). In this paper, there is a polarization diagram for an idealized two-level atom ($J_l = 3/2,\ J_u = 5/2$). The atomic species S II we consider has a ground level $J_l = 3/2$, but with three upper levels $J_u = 1/2$, 3/2, and 5/2. To benchmark our results, we also made a test calculation with only one upper level $J_u = 5/2$ and reproduced the result[7] in the aforementioned paper.

6. HANLE REGIME STUDIES: CIRCUMSTELLAR SCATTERING

The geometry of the system is given in Figure 13. We consider two cases. In the first case, a planar equatorial disk is expanding at a constant speed v (see Ignace et al. 1999). For a point in the disk (r, φ), the projected speed along the line of sight would be

$$v_z = v \sin i \cos\varphi. \tag{24}$$

The isovelocity zone is thus a pair of radial "spokes" at $\pm\varphi$, since the velocity v and the inclination i are constant.

In the second case, we consider a Keplerian disk. At a point (r, φ), the line-of-sight speed is

$$v_z = v(R)\sqrt{\frac{R}{r}} \sin i \sin\varphi. \tag{25}$$

Because of the differential rotation, the same polarized intensity along the same spoke will be distributed at a different frequency (or line-of-sight velocity). Oscillation thus appears in the observed signals (see Figs. 14 and 15).

We discuss two cases of magnetic configurations below, poloidal dipole field and toroidal field. In both cases, the radiation is perpendicular to the magnetic field, i.e., $\theta_r = 90^\circ$. Combining equations (13) and (16), we obtain the Stokes parameters for the emission from upper level $J_u = 3/2$,

$$\begin{aligned}
I &= \frac{\lambda^2}{4\pi} A I_* n \varrho_0^0 \Psi(\nu - \nu_0) 18.751\Gamma^2 + 1.1933 \sin^2\theta \sin 2(\phi - \phi_r)\Gamma \\
&\quad + 0.5967 \sin^2\theta \cos 2(\phi - \phi_r) - \cos^2\theta\left(1.8597\Gamma^2 + 0.465\right) + 4.6882, \\
Q &= \frac{\lambda^2}{4\pi} A I_* n \varrho_0^0 \Psi(\nu - \nu_0)\left\{\cos\theta \sin 2\gamma [2.3866\Gamma \cos 2(\phi_r - \phi) + 1.1933 \sin 2(\phi_r - \phi)]\right. \\
&\quad \left. + \cos 2\gamma \sin^2\theta\left(1.8597\Gamma^2 + 0.465\right) + \cos 2\theta \cos 2\gamma [0.5967\Gamma \sin 2(\phi_r - \phi) - 0.2983 \cos 2(\phi - \phi_r)]\right\}, \\
U &= \frac{\lambda^2}{4\pi} A I_* n \varrho_0^0 \Psi(\nu - \nu_0)\{1.1933 \cos 2\gamma \cos\theta [\sin 2(\phi - \phi_r) - 2\Gamma \cos 2(\phi - \phi_r)] \\
&\quad + 0.2983 \cos 2\theta \sin 2\gamma [\cos 2(\phi - \phi_r) + 2\Gamma \sin 2(\phi - \phi_r)]\},
\end{aligned} \tag{26}$$

where $\varrho_0^0 = \rho_0^0/(127.65\Gamma^2 + 31.91)$. The intensity of the incident radiation is $I_* = I_s(r/R_s)^2$, where I_s and R_s are the surface intensity and the radius of the central source, respectively.

[7] Apart from the minus signs of the Stokes parameters Q and U, which is due to a different choice of reference.

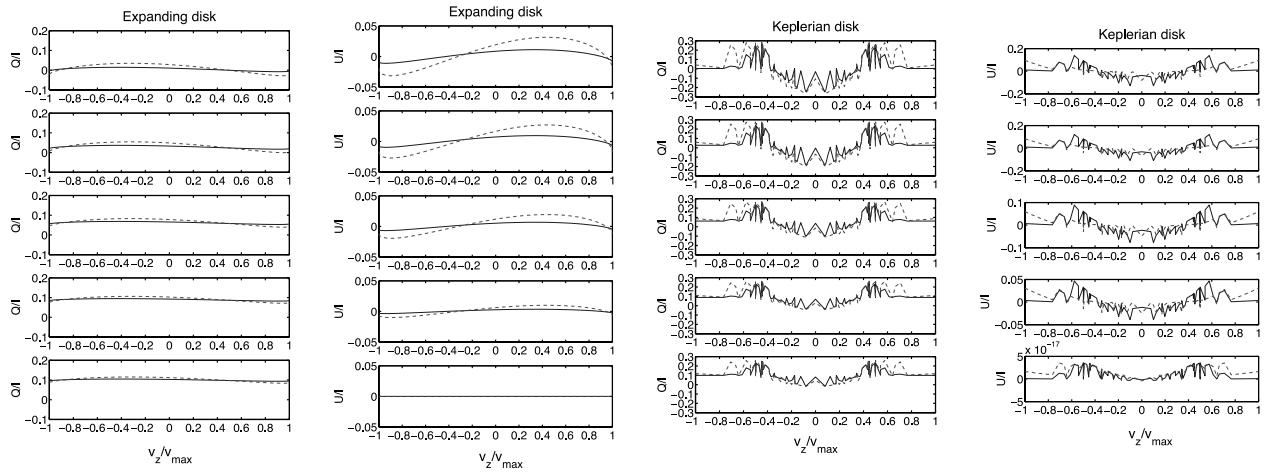

FIG. 14.—Linear polarizations vs. line frequency shift for disks with a dipole field, where $v_{\max} = v(R)\sin i$. The left two panels show the results for an expanding disk; the right two panels are for the Keplerian disk. The dashed line represents the result for $\Gamma'(R) = 0.01$, and the solid line is for $\Gamma'(R) = 0.1$. The inclinations are $i = 10^\circ, 30^\circ, 50^\circ, 70^\circ$, and 90° in the panels from top to bottom. [*See the electronic edition of the Journal for a color version of this figure*.]

6.1. *Poloidal Field*

First, let us consider the case of a dipole field. In the midplane, the field strength is

$$B = B_z = \frac{p_m}{r^3} = B(R)\left(\frac{R}{r}\right)^3, \tag{27}$$

where p_m is the magnetic dipole moment. The polarization at each v_z (or ϕ) is the summation of the contributions at different distances (r) along the same "spoke." The magnetic field is uniformly directed along the symmetry axis of the plane (see Fig. 13, *left*), thus $\theta_r = 90^\circ$ and $\phi_r = \varphi$. The angle between the line of sight and the magnetic field is equal to the viewing inclination $\theta = i$, and we define the ξ-ζ plane to be parallel to the line of sight, and thus, the azimuthal angle of the line of sight is $\phi = 0$. We choose the reference plane to be parallel to the ξ-ζ plane, i.e., $\gamma = 0$ (see Fig. 3, *right*). We consider five different viewing inclination angles, $i = 10^\circ, 30^\circ, 50^\circ, 70^\circ$, and 90°, and two different magnitudes of magnetic field, $\Gamma'(R) = 2\pi g_u \nu_L(R)/A = 0.01$ and 0.1. The results are given in Figure 14.

6.2. *Toroidal Field*

In the case of a toroidal field $B_\phi = B(R)R/r$, the direction of the field depends on the azimuthal angle φ. The theoretical frame defined by the magnetic field (see Fig. 13, *right*) varies from point to point along the "ring" (see Fig. 13, *right*). Consider a point (r, φ) on the "ring," the B field defines the z''-axis and we choose the radial direction to be the x''-axis. The radiation is then seen coming from $\theta_r = 90^\circ$, $\phi_r = 0^\circ$. The line of sight seen in the x'', y'', z'' frame is dependant on both the azimuthal angle φ and the inclination angle i. The detailed derivation of the geometric relation is given in the Appendix. We only provide the results here, $\theta = \cos^{-1}(-\sin i \sin\varphi)$, $\phi = \cos^{-1}(-\sin i \cos\varphi/\sin\theta)$. Since the magnetic fields are oriented in different directions, we adopt the plane defined by the symmetry axis and line of sight as the

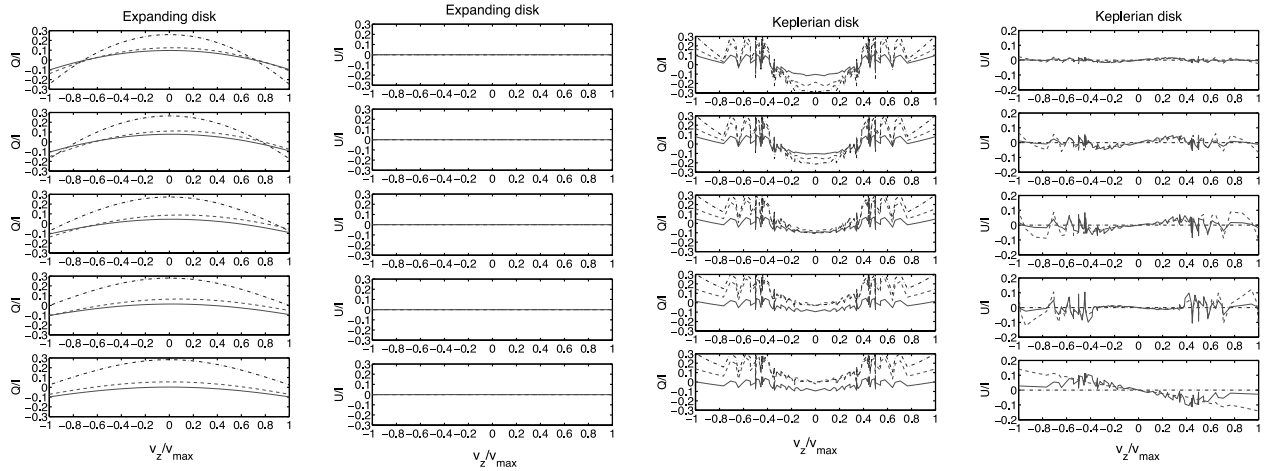

FIG. 15.—Linear polarizations vs. line-of-sight speed for disks with a toroidal field. The left two panels show the results for an expanding disk; the right two panels are for the Keplerian disk. The dashed line represents the result for $\Gamma'(R) = 0.1$, and the solid line is for $\Gamma'(R) = 1$. For comparison, we also plot the polarizations in the case of zero magnetic field (*dash-dotted lines*). The inclinations are $i = 10^\circ, 30^\circ, 50^\circ, 70^\circ$, and 90° in the panels from top to bottom. [*See the electronic edition of the Journal for a color version of this figure*.]

reference plane instead. The angle γ (see Fig. 3, *right*) between the two planes is equal to the angle between the magnetic field and the symmetry axis in the plane of sky. It can be proved (see the Appendix) that for $i \neq 90^\circ$,

$$\gamma = \cos^{-1}\left(\frac{\cos i \sin\varphi}{\sqrt{\cos^2 i \sin^2\varphi + \cos^2\varphi}}\right)\begin{cases} 1, & 0^\circ \leq \varphi \leq 90^\circ, \\ -1, & 90^\circ < \varphi \leq 180^\circ, \end{cases} \tag{28}$$

if $i = 90^\circ$ and $\gamma = 0^\circ$. The results for the five cases with the different inclination angles and two different field strengths $\Gamma'(R) = 0.1$ and 1 are given in Figure 15. Compared to Ignace et al. (1999), the major difference is the symmetry about the line center ($v_z = 0$) shift. Because of the inclination, we do not expect symmetry (see eq. [25]).

7. EFFECT OF ATOMIC ALIGNMENT ON RADIO AND FAR-INFRARED MAGNETIC DIPOLE LINES

7.1. *Formalism for Magnetic Dipole Lines*

The alignment on the ground state affects not only the optical (or UV) transitions to the excited state, but also the magnetic dipole transitions within the ground state. We briefly outlined this effect in YL07 using H I 21 cm and N V 70.7 mm lines. We provide here a more detailed discussion and its implications for the measurements. The 21 cm line is an important diagnostic, especially for the epoch of reionization. Indeed, Lyα pumping of H I has been extensively discussed in the literature, and the resulting 21 cm line is a powerful tool for studying the cosmological earlier epoch. Similar to H I, other species that have a structure within the ground state are also influenced by the optical pumping[8] through the Wouthuysen-Field effect (see Field 1958; Furlanetto et al. 2006 for a review). Recently, oxygen pumping has been proposed as a probe for the intergalactic metals at the epoch of reionization (Hernández-Monteagudo et al. 2007).

However, in all these studies the pumping light is assumed to be isotropic. This is problematic, particularly for the metal lines whose optical depth is small. During the early epoch of reionization, for instance, the ionization sources are localized, which introduces substantial anisotropy. The atomic alignment introduced by the anisotropy of the radiation field can play an important role in many circumstances. We shall show here this oversimplified approach can lead to a substantial error in the predictions.

In some sense, this study is similar to the case of the weak pumping regime discussed in YL06. But we take into account, in addition, the absorption and stimulated emission within the ground state owing to the presence of the CMB. The evolution equations of the occupation on the ground state can be obtained correspondingly by adding the absorptions and stimulated emissions to equations (27) and (28) in YL06,

$$\begin{aligned}\dot{\rho}_0^k(J_l^0) = &\sum_{J_l} p_k(J_l, J_l^0)[J_l]\left[A_m + B_m^s I_m\right]\rho_0^k(J_l) + \sum_{J_u} p_k(J_u, J_l^0)[J_u] A \rho_0^k(J_u) \\ &- \sum_{J_l} B_m I_m \rho_0^k(J_l^0) - \sum_{J_u,K,k'} (\delta_{kk'} B_{lu} \bar{J}_0^0 + s_{kk'}(J_u, J_l^0, 0, 0) B_{lu} \bar{J}_0^2)\rho_0^{k'}(J_l^0).\end{aligned} \tag{29}$$

For those lower levels other than the ground level,

$$\begin{aligned}\dot{\rho}_0^k(J_l) = &\sum_{J_l'} p_k(J_l', J_l)[J_l'](A_m|_{E'>E} + B_m^s|_{E'>E} I_m + B_m|_{E'<E} I_m)\rho_0^k(J_l') \\ &+ \sum_{J_u} p_k(J_u, J_l)[J_u] A \rho_0^k(J_u) - \sum_{J_l'} \left(A_m|_{E>E'} + B_m^s|_{E>E'} I_m + B_m|_{E<E'} I_m\right)\rho_0^k(J_l).\end{aligned} \tag{30}$$

In the above equations, A_m, B_m, and B_m^s respectively represent the spontaneous emission, absorption, and stimulated emission coefficients, and I_m is the corresponding radiative intensity. For the intergalactic medium, the microwave intensity I_m is usually given by CMB, which by its nature is isotropic.[9] If the splitting of the ground state is owing to fine structure, the equivalent temperature T_* of the energy separation of the first metastable level (J_l^1) from the ground level (J_l^0) is usually much larger than the CMB temperature so that a two-level model involving only the ground level (J_l^0) and the first metastable level (J_l^1) would be adequate. We also neglected the optical pumping from level J_l^1, which is much smaller than the pumping from level J_l^0. Combined with the evolution equation of the upper level (J_u, eq. [1]), we then obtain

$$\begin{aligned}&\sum_{J_u,k'} BI_\nu \left\{ \left[J_u, J_l^0\right] p_k\left(J_u, J_l^0\right) \frac{A\left(J_l^0\right)}{\sum_{J_l''} A''} \left[\delta_{kk'} p_k\left(J_u, J_l^0\right) + r_{kk'}\left(J_u, J_l^0, 0, 0\right)\frac{\bar{J}_0^2}{\bar{J}_0^0}\right] - \left[\delta_{kk'} + s_{kk'}\left(J_u, J_l^0, 0, 0\right)\frac{\bar{J}_0^2}{\bar{J}_0^0}\right]\right\}\rho_0^{k'}\left(J_l^0\right) \\ &+ p_k\left(J_l^0, J_l\right)[J_l]\left(A_m + B_m^s I_m\right)\rho_0^k(J_l) - B_m I_m \rho_0^k\left(J_l^0\right) = 0,\end{aligned} \tag{31}$$

$$\begin{aligned}&\left[A_m + B_m^s I_m\right]\rho_0^k(J_l) = p_k\left(J_l^0, J_l\right)\left[J_l^0\right]\rho_0^k\left(J_l^0\right) \\ &+ BI_\nu \sum_{J_u,k'} \frac{A(J_l)}{\sum_{J_l''} A''} p_k(J_u, J_l)\left[J_u, J_l^0\right]\left[\delta_{kk'} p_{k'}\left(J_u, J_l^0\right) + r_{kk'}\left(J_u, J_l^0, 0, 0\right)\frac{\bar{J}_0^2}{\bar{J}_0^0}\right]\rho_0^{k'}\left(J_l^0\right),\end{aligned} \tag{32}$$

[8] To clarify, we do not distinguish between pumping by optical lines or UV lines and name them universally optical pumping.
[9] Therefore, it does not have the dipole component, unlike the optical pumping light.

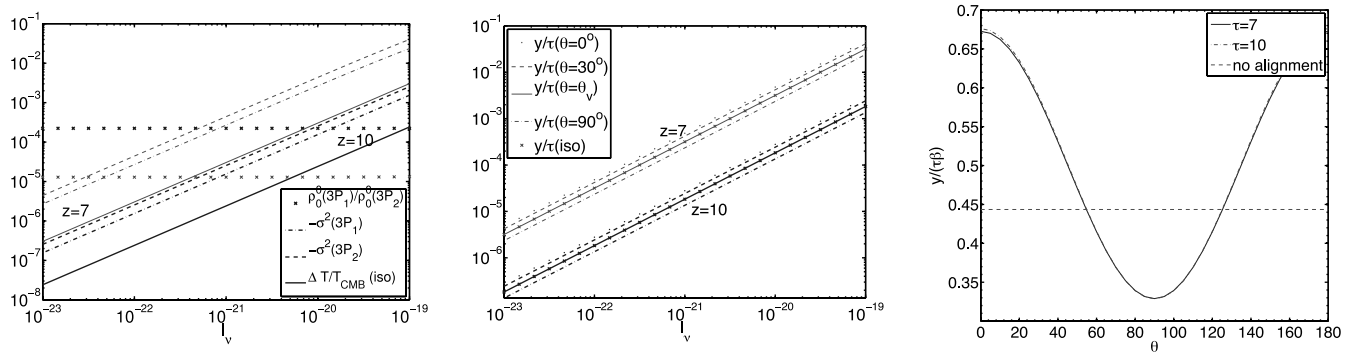

FIG. 16.—*Left*: Density matrices of the first metastable level $3P_1$ and the ground level $3P_2$ of O I. *Middle*: Distortion of CMB due to the anisotropic pumping of O I at redshifts $z = 7$ and 10. While the temperature distortion (eq. [36]) almost agrees with the result for isotropic pumping apart from a constant factor, the distortion in the intensity (eq. [40]) is influenced by the anisotropy of the radiation and the atomic alignment. Only when the angle between the line of sight and the pumping radiation approaches the Van Vleck angle, $\theta_V = 54.7°, 180° - 54.7°$, does the result agree with the isotropic pumping. *Right*: Distortion of CMB y/τ is proportional to β. The ratio $y/(\tau\beta)$ thus only varies with the angle between the line of sight and the pumping radiation due to atomic alignment. The alignment can cause a variation of y/τ up to a factor of 2. The case without alignment accounted for is also plotted for comparison (*dashed line*). [*See the electronic edition of the Journal for a color version of this figure.*]

where $I_m = B_{\nu(J_l \to J_l^0)}(T)$ is the blackbody radiative intensity at temperature T. For simplicity, we dropped the index "1" for the first metastable level and refer to it as J_l. For many lines $T_* \gg T$, so the excitation and stimulated emission for the magnetic dipole transition within the ground state is much slower than the corresponding emission rate. Define $\beta = BI_\nu/B_m I_m$. When $\beta \gg 1$, the absorption and stimulated emission can be neglected (the terms containing the factor I_m), and the above equations reduce to the expressions we obtained in YL06 for the weak pumping case. If β gets to the order of unity, however, all the magnetic dipole transitions within the ground state should be accounted for, and the above equations should be applied. The occupation on the ground state is in general determined by the two factors β and $\bar{J}_0^2(\theta_r)/\bar{J}_0^0$ (eq. [6]). If there is no magnetic field, we can choose the quantization axis along the direction of the UV radiation so that $\theta_r = 0$ (see Fig. 1, *right*). In this case, the factor $\bar{J}_0^2/\bar{J}_0^0 = W_a/(\sqrt{2}W)$ is solely determined by the anisotropy. We obtain from equations (31) and (32)

$$\frac{\rho_0^0(J_l)}{\rho_0^0(J_l^0)} = \frac{\sqrt{[J_l^0]}B_m I_m}{\sqrt{[J_l]}(A_m + B_m^s I_m)}\left\{\beta\left[1 - \frac{A(J_l^0)}{\sum_{J_l''} A''}\right] + 1\right\},$$

$$\rho_0^2(J_l) \simeq \frac{\beta B_m I_m}{A_m + B_m^s I_m}\sum_{J_u}\frac{A(J_l)}{\sum_{J_l''} A''} p_2(J_u, J_l)\left[J_u, J_l^0\right] r_{20}\left(J_u, J_l^0, 0, 0\right)\frac{\bar{J}_0^2}{\bar{J}_0^0}\rho_0^0\left(J_l^0\right),$$

$$\rho_0^2(J_l^0) \simeq \sum_{J_u}\beta\left[\left[J_u, J_l^0\right]\frac{A(J_l^0)}{\sum_{J_l''} A''} r_{20}\left(J_u, J_l^0, 0, 0\right)\frac{\bar{J}_0^2}{\bar{J}_0^0}\left(p_2\left(J_u, J_l^0\right) + [J_l]\, p_2\left(J_l^0, J_l\right)p_2(J_u, J_l)\right) - s_{20}\left(J_u, J_l^0, 0, 0\right)\frac{\bar{J}_0^2}{\bar{J}_0^0}\right]\rho_0^0\left(J_l^0\right). \quad (33)$$

In many cases, it is useful to quantify the level population by the spin temperature,

$$\frac{n(J_l)}{n\left(J_l^0\right)} = \frac{[J_l]}{\left[J_l^0\right]}\exp\left(-\frac{T_*}{Ts}\right), \quad (34)$$

where $n(J) = N\sqrt{[J]}\rho_0^0(J)$. Combined with equation (33), the above equation yields

$$\exp\left(-\frac{T_*}{Ts}\right) = \frac{\left[J_l^0\right]B_m I_m}{[J_l](A_m + B_m^s I_m)}\left\{\beta\left[1 - \frac{A\left(J_l^0\right)}{\sum_{J_l''} A''}\right] + 1\right\}. \quad (35)$$

7.2. *Anisotropic Pumping of* [O I] *63.2* μm

Here we use O I as an example to demonstrate the effect of atomic alignment on the radio diagnostics based on magnetic dipole transitions within the ground state. A comparison with the recent work on oxygen pumping in the high-redshift intergalactic medium will be provided. For O I, their fine structure is illustrated in Figure 6. In Table 4, we list the corresponding coefficients p_k, $r_{kk'}$, and $s_{kk'}$ (eqs. [1]–[3]).

Given these parameters, the linear equations (31) and (32) can be easily solved to get the density matrices for the two sublevels $J_l = 1$ and 2. As shown in Figure 16 (*left*), the total population among the sublevels is marginally affected by the UV pumping. The spin temperature we obtain, however, differs from the result of Hernández-Monteagudo et al. (2007) by a numerical factor 4/3. This difference arises from the existence of the second metastable level $J_l = 0$. In Hernández-Monteagudo et al. (2007), this level is completely neglected. In reality, the atoms pumped from the ground level $J_l^0 = 2$ to the excited state $^3S_1$ have a finite probability 1/9 of jumping to the level $J_l = 0$ as well as 1/3 probability of going to level $J_l = 1$. So the total probability of atoms leaving the level $J_l^0 = 2$ through optical pumping atoms would be $1/9 + 1/3 = 4/9$ rather than 1/3 in the two-level model adopted in Hernández-Monteagudo et al.

(2007). The deviation of the spin temperature from CMB $\Delta T/T_{\rm CMB}$ is proportional to the probability of the optical pumping rate from the ground level $J_l^0 = 2$ to other sublevels. Thereby, our result for $\Delta T/T_{\rm CMB}$ is 4/3 larger. From equation (35), we get

$$\frac{T_s - T_{\rm CMB}}{T_{\rm CMB}} = \frac{T_{\rm CMB}}{T_*}\,\exp\left(\frac{T_*}{T_{\rm CMB}}\right)\left[1 - \frac{A(J_l^0)}{\sum_{J_l} A(J_l)}\right]\frac{[J_l^0]\beta B_m I_m}{[J_l](A_m + B_m^s I_m)}, \tag{36}$$

where $I_m = B_{63.2\ \mu{\rm m}}(T_{\rm CMB}(z))$ is given by the CMB.

The distortion in the CMB radiation is, however, influenced by the anisotropy of the radiation and the atomic alignment. This is because both emissivity and the absorption coefficient depend on the dipole component of the density matrix (see eqs. [9] and [13]). The ratio of the optical depth accounting for alignment to that without alignment is

$$\tilde{\tau} = \frac{\tau}{\tau_0} = \frac{\tilde{\eta} - \tilde{\eta}_{s,i}\exp(-T_*/T_s)}{1 - \exp(-T_*/T_s)}. \tag{37}$$

According to equations (9) and (13),

$$\tilde{\eta}_i = \eta_1/\eta_1^0 = 1 + w_{0l}\sigma_0^2(J_l^0)\mathcal{J}_0^2(i,\Omega), \tag{38}$$

$$\tilde{\eta}_{s,i} = \tilde{\epsilon}_i = \epsilon_i/\epsilon_i^0 = 1 + w_{l0}\sigma_0^2(J_l)\mathcal{J}_0^2(i,\Omega) \tag{39}$$

are the ratios of absorption and stimulated emission coefficients with and without alignment, where $\mathcal{J}_0^2(i,\Omega)$ is given by equation (4). As we see, unless the angle between the line of sight and the pumping radiation is equal to the Van Vleck angle $\theta_{\rm V} = 54.7^\circ, 180^\circ - 54.7^\circ$, a finite correction due to atomic alignment σ_0^2 would occur for the optical depth. Equation (33) indicates that $\sigma_0^2(J_l)$ and $\sigma_0^2(J_l^0)$ are proportional to β and $\rho_0^0(J_l)/\rho_0^0(J_l^0)$ is only sensitive to $T_{\rm CMB}$ in the case of $\beta \ll 1$ (see Fig. 16).

The distortion from the CMB can be obtained using the radiative transfer equation $dI/ds = h\nu\Psi(\nu)/4\pi[n_l(A_m + B_m I_m) - n_0 B_m^s I_m]$. In the optically thin case $\tau \ll 1$,

$$\begin{aligned} y = \frac{\Delta I_\nu}{B_\nu(T_{\rm CMB})} &= \tau\left\{\frac{\tilde{\epsilon}_0[\exp(T_*/T_{\rm CMB}) - 1]}{\tilde{\eta}\exp(T_*/T_s) - \tilde{\eta}_s} - 1\right\} \\ &= \tau_0\left\{\frac{\tilde{\epsilon}_0[\exp(T_*/T_{\rm CMB}) - 1]}{\exp(T_*/T_s) - 1} - \tilde{\tau}\right\} \\ &\simeq \tau_0[\tilde{\epsilon}_0(1 + y_{\rm iso}/\tau_0) - \tilde{\tau}] \\ &= \tilde{\epsilon}_0 y_{\rm iso} + \tau_0\frac{[w_{l0}\sigma_0^2(J_l) - w_{0l}\sigma_0^2(J_l^0)](1 - 1.5\sin^2\theta)/\sqrt{2}}{1 - \exp(-T_*/T_s)}, \end{aligned} \tag{40}$$

where $y_{\rm iso}$ is the distortion neglecting the anisotropy of the radiation field and atomic alignment (see Hernández-Monteagudo et al. 2007). Indeed, if alignment is not accounted for, then

$$y = y_{\rm iso} = \tau_0\frac{T_*}{T_s}\frac{T_s - T_{\rm CMB}}{T_{\rm CMB}} = \tau_0\frac{T_{\rm CMB}}{T_s}\,\exp\left(\frac{T_*}{T_{\rm CMB}}\right)\left[1 - \frac{A(J_l^0)}{\sum_{J_l} A(J_l)}\right]\frac{[J_l^0]\beta B_m I_m}{[J_l](A_m + B_m^s I_m)}. \tag{41}$$

Both $\tilde{\eta}_s$ and $\tilde{\tau}$ depend on the line of sight and the atomic alignment (eqs. [37] and [39]); the resulting distortion in radiation is thus determined by the angle θ as well as the UV intensity of the O I line I_ν (or β, see eqs. [31] and [32]), which determines the atomic density and alignment (see Fig. 16). According to equation (33), $\sigma_0^2(J_l^0), \sigma_0^2(J_l) \propto \beta$. Since both of the terms on the right-hand side of equation (40) are proportional to β, the resulting distortion y is also proportional to β. Dividing $y\tau$ by β, we show the dependence on θ in Figure 16 (*right*).

7.3. *Magnetic Field in the Epoch of Reionization?*

The issue of magnetic field at the epoch of reionization is a subject of controversies. The fact that the levels of the O I ground state can be aligned through anisotropic pumping suggests to us a possibility of using atomic alignment to diagnose whether magnetic field exists at that early epoch. The degree of polarization in the optically thin case can be obtained in a similar way as above by replacing $\tilde{\eta}_0$ and $\tilde{\epsilon}_0$ by $\tilde{\eta}_1$ and $\tilde{\epsilon}_1$. In the alignment regime, the Stokes parameter $U = 0$, and therefore,

$$\begin{aligned} P = \frac{Q_\nu}{B_\nu(T_{\rm CMB})} &= \tau\left\{\frac{\tilde{\epsilon}_1[\exp(T_*/T_{\rm CMB}) - 1]}{\tilde{\eta}_1\exp(T_*/T_s) - \tilde{\epsilon}_1} - 1\right\} \\ &\simeq \tau_0\left[\tilde{\epsilon}_1\left(1 + \frac{y_{\rm iso}}{\tau_0}\right) - \frac{\tilde{\eta}_1 - \tilde{\epsilon}_1}{1 - \exp(-T_*/T_s)}\right] \\ &= \tilde{\epsilon}_1 y_{\rm iso} - \tau_0\frac{1.5\sin^2\theta[w_{l0}\sigma_0^2(J_l) - w_{0l}\sigma_0^2(J_l^0)]/\sqrt{2}}{1 - \exp(-T_*/T_s)}. \end{aligned} \tag{42}$$

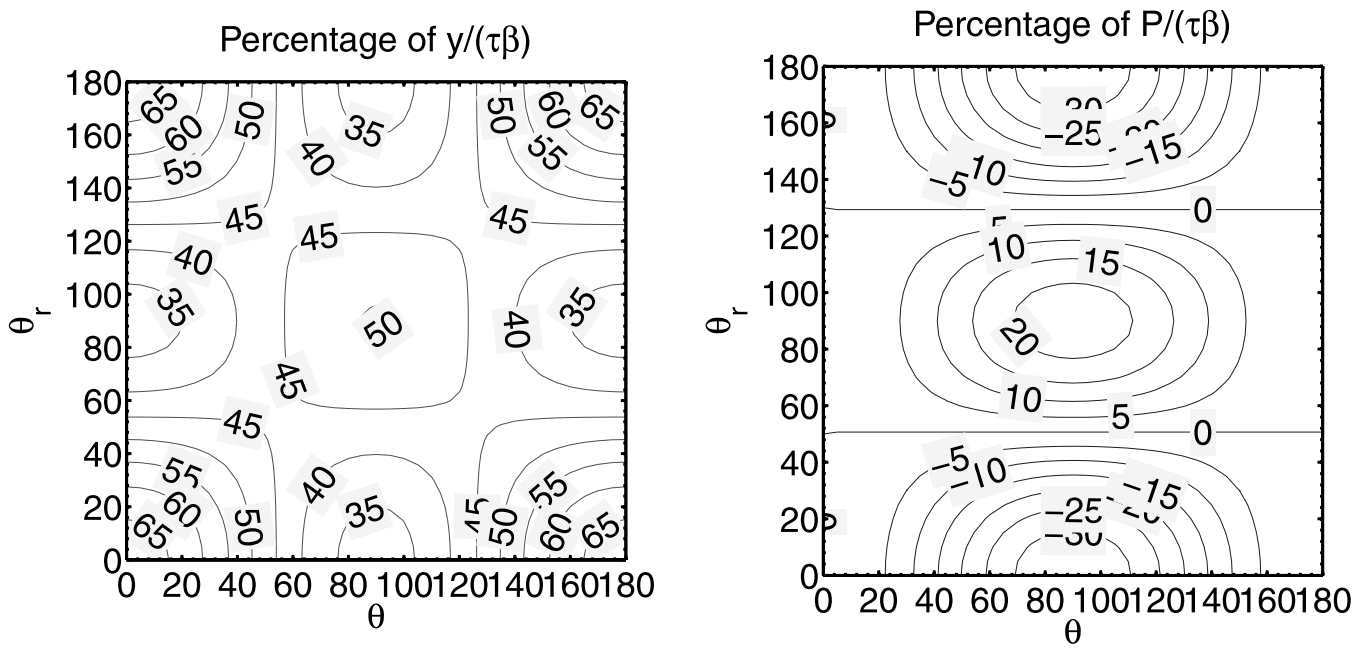

FIG. 17.—Contour plots of equal percentages of the ratios $y/(\tau\beta)$ and $P/(\tau\beta)$. The angles θ_r and θ are respectively the angles of the incident radiation and the line of sight from the magnetic field. [*See the electronic edition of the Journal for a color version of this figure*.]

In the case of nonzero magnetic field, the density matrices are determined by θ_r, the angle between magnetic field, as well as by the parameter β. Similar to y, the degree of polarization is also proportional to β. In Figure 17 we show the dependence of the ratios $y/(\tau\beta)$ and $P/(\tau\beta)$ on θ_r and θ. Since $U = 0$, the line is polarized either parallel ($P > 0$) or perpendicular ($P < 0$) to the magnetic field. The switch between the two cases happens at $\theta_r = \theta_V = 54.7^\circ, 180^\circ - 54.7^\circ$, which is a common feature of polarization from the aligned level (see YL06,YL07 for detailed discussions).

We discussed pumping of hyperfine lines [H I] 21 cm and [N V] 70.7 mm in YL07 and fine line [O I] 63.2 μm here. Certainly, this effect widely exists in all atoms with some structure on ground state, e.g., Na I, K I, fine-structure lines, [C I], [C II], [Si II], [N II], [N III], [O II], [O III], [S II], [S III], [S IV], [Fe II], etc. (see Table 4.1 in Lequeux 2005). Many atomic radio lines are affected in the same way, and they can be utilized to study the physical conditions, especially in the early universe: abundances, the extent of reionization through the anisotropy (or localization) of the optical pumping sources, *magnetic fields*, etc.

8. DISCUSSION

In this paper we extended our studies of atomic alignment in diffuse media. We provided more calculations of polarization of absorption lines arising from aligned species. We filled the gap of our earlier studies by considering the polarization of emission lines arising from aligned species with fine structure. In addition, we considered atomic alignment in the presence of the Hanle effect. By studying both the ground and upper state Hanle effects, we attempted to give a more comprehensive coverage of the diagnostic of the atomic resonant line on weak magnetic field in the diffuse circumstellar, interstellar, and intergalactic media.

8.1. *Previous Work on Atomic Alignment*

Let us briefly state some milestones in the studies of atomic alignment. A more detailed discussion is provided in YL06 and YL07. First of all, atomic alignment was studied in the laboratory in relation to early-day maser research (see Hawkins 1955).

In the astrophysical context, atomic alignment was proposed by Varshalovich (1968). The atomic alignment for an idealized atom with two levels and magnetic field directed along the line of sight was considered by Landolfi & Landi Degl'Innocenti (1986). We *benchmarked* our results by their calculations in the restricted geometry of observation. Polarization of emission lines arising from atomic pumping with mixing by magnetic field in the direction perpendicular to the symmetry axis of pumping radiation was considered in Lee et al. (1994). The radiation field there, nevertheless, is treated classically and we suspect that this cannot provide correct results. Originally, for the sake of simplicity, in Yan & Lazarian (2005) we attempted a similar approach motivated by the calculations in Hawkins (1955). However, our further studies proved that the results obtained without full QED treatment are erroneous, particularly for emission lines, as coherence among magnetic sublevels cannot be neglected. Our results for the polarization of the Na emission in YL07 differ from the corresponding results in Hawkins (1955).

Most of the research on the atomic alignment is done in the domain of solar physics.[10] This research, however, dealt with the atomic alignment in a regime, different from that important for the diffuse medium. The differences include the relative role of collisions, magnetic fields, and radiation. In particular, the Sun has radiation transfer effects that complicate the interpretation of the effects arising from

[10] Interestingly enough, our study shows that atomic alignment effects are more important for the diffuse medium, e.g., around luminous stars, where collisional depopulation is reduced compared to the Sun.

alignment, but are not so important for many circumstellar and interstellar species. For this reason we developed atomic alignment theory applicable for the diffuse astrophysical medium. Some of our results, e.g., polarization of absorption lines, do not have analogs in solar research. Because the alignable species and the regimes of alignment are different, we performed an extended program of calculation of alignment for a number of astrophysically important species. However, in the present paper we also benchmarked our codes by reproducing some results that were obtained by the solar community.

Extensive studies of polarization of absorption lines arising from atoms with fine structure submerged in weak magnetic field of an arbitrary direction are provided in YL06. The first studies of astrophysically important cases of atomic alignment for atoms with hyperfine structure in weak magnetic field of arbitrary direction are provided in YL07. This paper continues and extends these studies. Our approach can be applied to other problems, e.g., the ones discussed in Lee et al. (1994).

We stress the importance of taking into account magnetic fields while calculating the polarization. For instance, polarization of absorption arising from the atomic alignment is suggested as the mechanism of the observed polarization of Hα lines (Kuhn et al. 2007). However, the effect of magnetic field is neglected there, while our present study and earlier studies in YL06 and YL07 show that magnetic fields should be accounted for to get correct polarization measures.

8.2. *Studies of Stronger Magnetic Fields*

In our previous papers, we conducted an extensive study of atomic alignment and demonstrated their diagnostic power for weak magnetic field in diffuse media (e.g., in ISM). When field gets stronger than 1 G or so, the magnetic mixing becomes comparable to the line width; this is the domain of the Hanle regime. Originally defined as a modification of the polarization of resonant scattering, the Hanle effect has been known for decades. However, until recently (see Landi Degl'Innocenti 1999; Trujillo Bueno 1999), the alignment of the ground level and the effect of magnetic field on the ground level were not considered. Nevertheless, magnetic field is treated as a destructive factor to the ground level alignment. Magnetic field, in fact, realigns the atoms toward (either parallel or perpendicular to; see YL06) the magnetic field in addition to reducing the degree of alignment on the ground state. The possibility of using the effect to diagnose the direction of magnetic field as well as the magnetic field strength is not well explored.

In this paper, using S II as an example, we provided a comparative study of the Hanle effect with and without atomic alignment on the ground state. A notable effect of atomic alignment on the Hanle effect has been identified. The atomic alignment carries additional information about the direction of magnetic field, which would be veiled otherwise. And quantitative results are provided for a generic geometry, which enables the possibility of a precise study of both magnetic field strength and its three-dimensional direction. Indeed, there are four parameters even for a known radiation source, θ_0, θ_B, ϕ_B, and B field strength.

For the study of magnetic field in the circumstellar medium, the geometry of the system is clearer than in the ISM, namely, the direction of radiation is well defined. Three lines (they can be from the same species) are thus adequate to get all the information about the magnetic field.

We also consider the lower level Hanle regime, which occurs when the inverse of the lifetime on the ground level, the photon pumping rate [$9.8\times10^4(R_*/r)^2$, for pumping of S II $J_l\rightarrow J_u=5/2$ by an O star], becomes comparable to the magnetic precession rate $\nu_{\rm L}\simeq 88(B/G)$. This can happen for a strong pumping source, e.g., quasars and supernovae, or a relatively weak magnetic field. In this situation, the ground state is not aligned with respect to magnetic field. Neither the magnetic field nor the radiation field is a good quantization axis. As a result, coherence appears and the ground state density now resembles the upper state in the Hanle regime. *Absorption* from the ground state is modulated the same way as the emission in the Hanle regime. Both the degree and the direction of the polarization varies with the magnetic field. Unlike the solar case, *absorption* lines are readily available for the circumstellar and interstellar media. Furthermore, the upper level also gets the imprint of the magnetic field through excitation from the ground state. And therefore, the polarization of *emission* also carries the information of the magnetic field. Unfortunately, the polarization of emission in the lower level Hanle regime is not well separated from that in the Hanle regime in the polarization diagram. This entails some complexity for interpreting the observations. However, if we combine emission and absorptions or different species, we should be able to disentangle the two regimes and obtain the information about the magnetic field and the environment.

Absorption from atoms in the ground Hanle regime are, nevertheless, polarized in a *unique* way which can distinguish itself from the other two regimes. In the magnetic realignment regime or the Hanle regime, polarization of absorption can only be parallel or perpendicular to $\boldsymbol{B}$ in the plane of sky. In the ground Hanle regime, however, the polarization can be in any direction as in the case of emission. Thus, if the polarizations of multiplets are neither parallel nor perpendicular to each other, the region under study must be in the ground Hanle regime. The polarization of *absorption* lines is thus more informative.

Note that in this paper we consider the region where the radiation source is far enough to be treated as a point source. There is thus a substantial dilution of the radiation field so that the dilution factor $W\ll 1$. Thus, $B\bar{J}^0_0/A=[J_u]/[J_l]W/(e^{h\nu/k_{\rm B}T}-1)\ll 1$, meaning that the radiative pumping rate is thus much smaller than the spontaneous emission rate. The two regimes, namely, the Hanle regime ($\Gamma'\simeq 1$) and ground Hanle regime ($\Gamma'\simeq 1$), are well separated physically. For the same reason, we do not include forward scattering when treating the absorptions, since the scattering intensity $I_{\rm em}\propto\rho_u\propto\bar{J}^0_0$ is much smaller.

8.3. *Radio Emission Lines Influenced by Optical Pumping*

A new development of the theory here, which is considered neither in YL06 nor in YL07 nor in solar research, is the calculation of the magnetic dipole transitions between the sublevels of the ground state, provided that the atoms are subject to *anisotropic* optical pumping. We provided calculations for O I transitions, but our approach is applicable to various atoms with hyperfine or fine splitting of levels. We showed that the emission arising from such atoms is polarized, which provides a new way of studying magnetic fields. For instance, in YL07 we studied the variations of 21 cm transmission arising from the alignment of H I atoms. Our present paper predicts that the transmission within the fine splitting of levels will be polarized. Apart from apparent Galactic and extragalactic applications, this may be an interesting process to study magnetic fields at the epoch of reionization, which hopefully will be available with the instruments that are currently under construction.

As for our study of O I pumping, we obtained, first of all, a factor of 4/3 correction for the $\Delta T/T_{\rm CMB}$ and $\Delta I_\nu/B_\nu(T_{\rm CMB})$ in the case of isotopic pumping of O I 63.2 μm compared to the earlier study by Hernández-Monteagudo et al. (2007). We also showed that in the realistic pumping by O I Balmer α lines, the anisotropy can introduce a factor of 2 variation in the resulting $\Delta T/T_{\rm CMB}$ and $\Delta I_\nu/B_\nu(T_{\rm CMB})$. Only when the angle between the line of sight and the incident radiation is 54.7° (the so-called Van Vleck angle), the results are coincident with those from isotropic pumping. These are important changes to be taken in modeling of the corresponding processes, as O I is being used to study processes in the early universe. More importantly, we predicted that the arising emission is polarized with a high degree of polarization (up to 30%). This provides a unique opportunity to trace magnetic fields in the early universe and also gauge the degree of reionization that arises from anisotropic optical pumping.

8.4. *Wide Extent of Alignment Effects*

In our studies we were focused on the new ways to study magnetic field that the atomic alignment of the atoms/ions with fine and hyperfine structures provides. Being alignable in their ground state, these species can be realigned in weak magnetic fields, which is extremely good news for the studies of weak magnetic fields in astrophysical diffuse gas. The latter studies are currently very limited, with polarimetry based on grain alignment being the most widely used technique (see Whittet 2005 and references therein). However, in spite of the progress of grain alignment theory (see Lazarian 2007 for a review), the quantitative studies of magnetic fields with aligned atoms are not always possible. Atoms, unlike dust grains, have much better defined properties, which allows, for instance, tomography of magnetic fields by using different species,[11] which would be differentially aligned at different distances from the source. In addition, ions can trace magnetic fields in the environments in which grains cannot survive. In fact, rather than compare advantages and disadvantages of different ways of studying magnetic fields, we would stress the complementary nature of different ways of conducting magnetic field studies. The subject is starved for both data and new approaches to getting the data. Note that atomic realignment happens on the Larmor precession time, which potentially allows one to study the dynamics of fast variations of magnetic fields, e.g., related to MHD turbulence.

An incomplete list of objects where the effects of alignment should be accounted for arises from our studies, which include this paper, as well as YL06 and YL07. These include diffuse media in the early universe, quasars, AGNs, reflection nebulae, high- and low-density ISM, circumstellar regions, accretion disks, and comets. One can easily add more astrophysical objects to this list. For instance, Io's sodium tail can be studied the same way as the sodium tail of comets. In general, in all environments when optical pumping is fast compared with the collisional processes we expect to see the effects of atomic alignment and magnetic realignment of atoms. The wide variety of atoms with fine and hyperfine structure of levels ensures multiple ways that the information can be obtained. Comparing information obtained through different species, one can get deep insights into the physics of different astrophysical objects. If the implications of atomic alignment influenced the understanding of particular features of the solar spectrum, then the studies of atomic alignment in diffuse astrophysical media can provide much deeper and yet unforeseen changes in our understanding of a wide variety of physical processes.

We note that it is also important that some atoms do not demonstrate the effects of alignment. A comparison of the properties demonstrated by these atoms with those that demonstrate the alignment allows one to gauge the importance of the effects of alignment. In addition, we would like to stress that the effects of atomic alignment are not limited by tracing all important astrophysical magnetic fields. As we discussed in YL06, YL07, and this paper, the variations of the optical/UV absorptions and emissions induced by atomic alignment may be really appreciable and may substantially influence the interpretation of the absorption lines in terms of element abundances. Our present study of the effects of alignment for the radio lines further extends the range of the effects for which a key role can be played by atomic alignment. This proves that further study of the effects of atomic alignment are necessary if we want to correctly interpret numerous pieces of observational data.

9. SUMMARY

Our results can be briefly summarized as follows.

1. Our calculations of more absorption lines arising from species aligned by weak magnetic field exhibit substantial degrees of polarization. Some of the atoms exhibit polarization that can be measured by ground-based observations.
2. Our calculations of the polarization of the emission lines arising from species aligned by weak magnetic field show that such studies are promising for magnetic field studies in diffuse media.
3. We discuss the situation when both the magnitude and the direction of weak magnetic fields in the diffuse gas can be studied. We show that this happens when the photon pumping rate becomes comparable to the magnetic precession rate; the coherence occurs in the ground level (ground state Hanle effect).
4. Dealing with the stronger magnetic field regime, i.e., when the upper level Hanle effect is important, we show that the polarizations of emission lines in the Hanle regime are affected by the ground state alignment and must be taken into account. At the same time, we show that the polarizations of absorption lines remain the same in the Hanle regime as in the atomic alignment regime.
5. Our calculations of the intensity ratio of scattered lines or absorption lines also varies in both the upper level Hanle and lower level Hanle regimes and, therefore, also carry the information about the direction of magnetic field.
6. We show that combining the Hanle effect, atomic alignment, and the lower level Hanle effect allows one to acquire a tomography of magnetic field for a variety of environments.
7. We demonstrate that atomic alignment can influence the emission of radio lines arising from optical pumping. Therefore, the anisotropic nature of the pumping radiation should be taken into account.

[11] As we discussed in YL06, long-lived alignable metastable states that are present for some atomic species between the upper and ground states may act as proxies of the ground states. The lifetime of the metastable level may determine the distance from the source over which the atoms are aligned on the metastable level. Absorption from such metastable levels can be used as a diagnostic for magnetic field in the vicinity of the star.

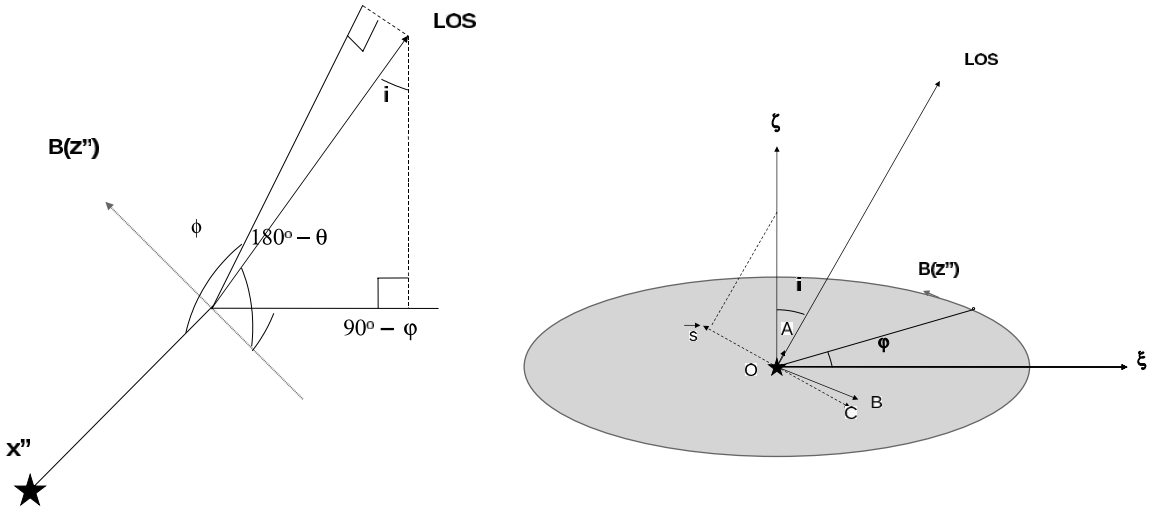

FIG. 18.—*Left*: Direction of the line of sight seen in the magnetic frame (θ, ϕ). *Right*: Vector $\boldsymbol{s}$ is the projection of the ζ-axis in the plane of sky and $-\boldsymbol{OC}$ is the projection of magnetic field in the plane of sky. The angle γ between the projections of the magnetic field and the disk symmetry axis ζ in the plane of sky is thus the angle between $\boldsymbol{s}$ and $-\boldsymbol{OC}$. [*See the electronic edition of the Journal for a color version of this figure*.]

8. The polarization of the radio lines can be used to study magnetic fields in the situations when other techniques fail, e.g., in the universe at the epoch of reionization.

9. With many species affected by atomic alignment and with a wide variety of effects that atomic alignment (and realignment) involves, we conclude that both the proper accounting for these effects is essential in modeling and that studies of the consequences of the alignment will open new ways to study physical processes in many astrophysical objects.

We are grateful to Ken Nordsieck for valuable comments and suggestions. H. Y. is supported by CITA and the National Science and Engineering Research Council of Canada. A. L. is supported by the NSF Center for Magnetic Self-Organization in Astrophysical and Laboratory Plasmas as well as NSF grant AST 05-07164 and NASA grant X5166204101.

APPENDIX

GEOMETRIC RELATIONS IN TOROIDAL DISK

In a toroidal disk, the magnetic field is changing direction from place to place. A transformation of the angles from place to place is thus necessary. Basically, three angles are needed, two angles $(\theta, \phi$; see Fig. 3, *right*) specifying the direction of the line of sight in the magnetic frame and the angle γ defining the reference plane for the polarization.

Since the line of sight is in the ξ-ζ plane (see Fig. 13, *right*), which is perpendicular to the disk, the angle between the line of sight and magnetic field θ is related to the inclination angle i and the angle φ by the relation (see Fig. 18, *left*)

$$\cos\theta = -\cos(90^\circ - i)\cos(90^\circ - \varphi). \tag{A1}$$

Similarly, it can be verified that the cosine of the angle between the line of sight and the x-axis is

$$\sin\theta\cos\phi = -\sin i\cos\varphi, \tag{A2}$$

thus, $\theta = \cos^{-1}(-\sin i\sin\varphi)$ and $\phi = \cos^{-1}(-\sin i\cos\varphi/\sin\theta)$.

We choose the ξ-ζ plane defined by the line of sight and the symmetry axis of the disk as the reference plane for measuring the positional angle of the line polarization; the angle γ between this plane and the magnetic field in the plane of sky (see Fig. 3, *right*) is then equal to the angle between the projections of the symmetry axis and magnetic field in the plane of sky. As shown in Figure 18 (*right*), the unit vector $\boldsymbol{s} = (-\cos i, 0, \sin i)$ is the projection of the ζ-axis in the plane of sky and $-\boldsymbol{OC}$ is the projected magnetic vector in the plane of sky. The angle γ between the two vectors is

$$\cos^{-1}\left(-\frac{\boldsymbol{s}\cdot\boldsymbol{OC}}{|OC|}\right). \tag{A3}$$

It can be seen that

$$\boldsymbol{OC} = \boldsymbol{OB} - \boldsymbol{OA}, \tag{A4}$$

where $\boldsymbol{OB}$ is the unit vector antiparallel to the magnetic field $\boldsymbol{OB} = (\sin\varphi, -\cos\varphi, 0)$, and $\boldsymbol{OA}$ is its projection $\boldsymbol{OA} = \sin i \sin\varphi(\sin i, 0, \cos i)$. Inserting them and the expression of $\boldsymbol{s}$ into equations (A3) and (A4), we obtain

$$\gamma = \cos^{-1}\left(-\frac{\sin\varphi\cos i}{\sqrt{\sin^2\varphi\cos^2 i + \cos^2\varphi}}\right). \tag{A5}$$

REFERENCES

Bertout, C. 1989, ARA&A, 27, 351
Bohr, N. 1924, Naturwissenschaften, 12, 1115
Bommier, V. 1977, Ph.D. thesis, Paris VI Univ.
———. 1980, A&A, 87, 109
Bommier, V., & Sahal-Brechot, S. 1978, A&A, 69, 57
Camenzind, M. 1990, Rev. Mod. Astron., 3, 234
Cameron, A. C., & Campbell, C. G. 1993, A&A, 274, 309
Field, G. B. 1958, Proc. IRE, 46, 240
Furlanetto, S. R., Oh, S. P., & Briggs, F. H. 2006, Phys. Rep., 433, 181
Gordon, K. D., et al. 2000, ApJ, 544, 859
Grandi, S. A. 1975, ApJ, 196, 465
Hanle, W. 1924, Z. Phys., 30, 93
Hawkins, W. B. 1955, Phys. Rev., 98, 478
Heisenberg, W. 1925, Z. Phys., 31, 617
Hubrig, S., Pogodin, M. A., Yudin, R. V., Schöller, & Schnerr, R. S. 2007, A&A, 463, 1039
Ignace, R., Cassinelli, J. P., & Nordsieck, K. H. 1999, ApJ, 520, 335
Johns-Krull, C. M., Valenti, J. A., & Koresko, C. 1999, ApJ, 516, 900
Königl, A. 1991, ApJ, 370, L39
Kuhn, J. R., Berdyugina, S. V., Fluri, D. M., Harrington, D. M., & Stenflo, J. O. 2007, ApJ, 668, 63L
Landi Degl'Innocenti, E. 1982, Sol. Phys., 79, 291
———. 1983, Sol. Phys., 85, 3
———. 1984, Sol. Phys., 91, 1
———. 1999, in Solar Polarization, ed. K. N. Nagendra & J. O. Stenflo (Boston: Kluwer), 61
Landolfi, M., & Landi Degl'Innocenti, E. 1985, Sol. Phys., 98, 53
———. 1986, A&A, 167, 200
Lazarian, A. 2007, J. Quant. Spectrosc. Radiat. Transfer, 106, 225
Lee, H.-W., Blandford, R. D., & Western, L. 1994, MNRAS, 267, 303
Lequeux, J. 2005, The Interstellar Medium (Berlin: Springer)
Hernández-Monteagudo, C., Rubiño-Martín, J. A., & Sunyaev, R. A. 2007, MNRAS, 380, 1656
Morton, D. C. 1975, ApJ, 197, 85
Shu, F. H., Njita, J., Ostriker, E., Wilkin, F., Ruden, S., & Lizano, S. 1994, ApJ, 429, 781
Stenflo, J. O. 1994, Solar Magnetic Fields: Polarized Radiation Diagnostics (Dordrecht: Kluwer)
Stenflo, J. O., & Keller, C. U. 1997, A&A, 321, 927
Trujillo Bueno, J. 1999, in Solar Polarization, ed. K. N. Nagendra & J. O. Stenflo (Boston: Kluwer), 73
Trujillo Bueno, J., Landi Degl'Innocenti, E., Casini, R., & Martínez Pillet, V. 2005, in Proc. Int. Sci. Conf. on Chromospheric and Coronal Magnetic Fields, ed. D. E. Innes, A. Lagg, & S. K. Solanki (ESA SP-596; Noordwijk: ESA), 4
Varshalovich, D. A. 1968, Astrofizika, 4, 519
———. 1970, Soviet Phys., 13, 429
Whittet, D. C. B. 2005, in ASP Conf. Ser. 343, Astronomical Polarimetry: Current Status and Future Directions, ed. A. Adamson et al. (San Francisco: ASP), 321
Yan, H., & Lazarian, A. 2005, in ASP Conf. Ser. 343, Astronomical Polarimetry: Current Status and Future Directions, ed. A. Adamson et al. (San Francisco: ASP), 346
———. 2006, ApJ, 653, 1292 (YL06)
———. 2007, ApJ, 657, 618 (YL07)